Diploma Thesis

FLURE - A Point-of-Care Fluorescence Lateral Flow Immunoassay Reader

submitted in satisfaction of the requirements for the degree of
Diplom-Ingenieur
of the TU Wien, Faculty of Electrical Engineering

Diplomarbeit

FLURE - Ein Point-of-Care Fluoreszenz Lateral Flow Immunoassay Lesegerät

ausgeführt zum Zwecke der Erlangung des akademischen Grades einer
Diplom-Ingenieurin
eingereicht an der Technischen Universität Wien, Fakultät für Elektrotechnik

von

Anne Schuchanegg, BSc

Matr.Nr.: 01404983

unter der Anleitung von

Ao.Univ.Prof. Dipl.-Ing. Dr.techn. **Franz Keplinger** (TU Wien)

Dipl.-Ing. **Christoph Aschl** (Bloom Diagnostics)

Institut für Elektrotechnik und Informationstechnik
Forschungsbereich Biomedical Engineering
Technische Universität Wien
Gußhausstraße 25-29, 1040 Wien, Österreich

Wien, am 21.2.2023 _____

ZUSAMMENFASSUNG

Die Zukunft des Gesundheitswesens liegt in der Heimdiagnostik, die durch den Mangel an medizinischem Personal und dem schnelllebigen Alltag der Patient*innen vorangetrieben wird. Bereits erhältliche mobile Testsysteme, die Blutwerte quantitativ analysieren, nutzen meist Tests, die auf Gold-Nanopartikeln basieren und durch dieses Ausleseverfahren in ihrer Sensitivität eingeschränkt sind. Fluoreszenzbasierte Tests und Analysegeräte bieten eine Alternative und lösen das Sensitivitätsproblem. In dieser Diplomarbeit wurden die Parameter eines solchen Gerätes, wie die Lichtquelle, der Lichtpfad, sowie alle Materialien innerhalb dieses Lichtpfades, wie die Testmembran und das Material der Testkassette optimiert, um damit einen Ausbau der Bloom Lab FLURE Technologie zu ermöglichen.

Verschiedene LEDs wurden mit Hilfe von drei Prototypen und einem speziell gefertigten Testaufbau, der "Experimental Unit", auf ihre Fähigkeit, mit fluoreszenten Partikeln versehene Teststreifen anzuregen, getestet. Auch die optimale Positionierung der LEDs wurde mit der Experimental Unit ermittelt. Es wurden drei verschiedene Testkassetten und sieben Kombinationen an Testmembranen und entsprechender Trägerkarte untersucht, um die geeignetsten Materialien zu bestimmen und die Autofluoreszenz zu minimieren.

Die besten Resultate wurden mit einer LED mit einer Spitzenwellenlänge von 365 nm und einem Abstrahlwinkel von 35° erzielt, die in einem Winkel von 0° direkt über dem Teststreifen positioniert wurde. Durch das Verwenden eines Langpassfilters, beginnend bei 475 nm, und einer schwarzen Testkassette konnte der Bildkontrast zusätzlich erhöht werden. Die Autofluoreszenz und das Reflexionsvermögen der verschiedenen Testmembranen zeigte sich unabhängig von der absoluten Porengröße, aber stark beeinflusst durch die Wahl der Trägerkarte. Testmembranen mit weißer Trägerkarte können aufgrund der starken, von ihnen verursachten Reflexion nicht mit der aktuellen Version des FLURE Labs verwendet werden.

Die Schlussfolgerung dieser Diplomarbeit ist, dass alle zukünftigen Entwicklungen des Bloom FLURE Labs auf den Parametern von Prototyp 3 aufbauen sollten, da dieses Modell die bereits oben genannten Eigenschaften zur Beleuchtung vereint. Prototyp 3 ermöglicht außerdem die Analyse von kommerziell erhältlichen, fluoreszenzbasierten Teststreifen anderer Hersteller, was großes Potential für den zukünftigen Markt bringt.

ABSTRACT

Home-based diagnostics is the future of healthcare, fueled by the lack of medical personnel and the busy lifestyle of patients. Mobile testing systems for quantitative analysis of different blood markers are already available on the market but as most of these read-out systems are based on gold nanoparticles they are limited in sensitivity. Fluorescence-based tests and readers offer a solution to these limitations. In this thesis, parameters of a fluorescent reader, like the light source and light path, as well as materials within the light path, namely immunoassay membrane and test cassette material were optimized to allow for further investigation of the Bloom Lab FLURE technology.

LEDs were tested in three different prototypes and in a custom-made test set-up, the "experimental unit", regarding their capability to excite fluorescently-labeled test strips. The experimental unit was also used to investigate ideal LED position. Three different test cassette materials and seven different combinations of lateral flow membranes and corresponding backings were tested to find the best option in regards to autofluorescence.

The best results were achieved using an LED at 365 nm peak wavelength with a relatively small viewing angle of 35° being positioned at 0° angle above the test strip. Contrast was further improved by addition of an optical longpass filter starting at 475 nm and the use of a black test cassette material. The autofluorescence comparison of different test membranes showed no correlation between pore size and reflectance or autofluorescence but found a strong dependence on the type of backing card. Lateral flow membranes with white backing cannot be used with the current version of the FLURE Lab due to high reflectance.

The final conclusion of this thesis is that future development should be based on Bloom FLURE Lab Prototype 3 which combines all parameters regarding the illumination as mentioned above. With this reader, analysis of commercially available fluorescence-based lateral flow tests is possible which offers great potential on the market.

Contents

List of Figures

List of Abbreviations

ABS Acrylonitrile butadiene styrene

ABSB Black ABS test cassette

ABSW White ABS test cassette

AuNP Gold nanoparticle

BG Background

CCD Charge-coupled device

CL Control line

CMOS Complementary metal-oxide-semiconductor

CNxx Cellulose nitrate mebrane by Sartorius

Covid-19 Coronavirus disease 2019

CRP C-reactive protein

Eu^{3+} Europium-ion

FFxx Cellulose nitrate membrane by Cytiva

FLURE Fluorescent read-out, project name

FWHM Full width at half maximum

G4, G7 Reference test strips

GG475, LP475 Long-pass filter with cut-on wavelength of 475 nm

HCG Human chorionic gonadotropin

HFxx Cellulose nitrate membrane by Millipore

IU/ml International unit per microliter

LED Light-emitting diode

LFIA Lateral flow immunoassay

MAKR Makrolon test cassette

MGV Mean-gray value

NP Nanoparticle

NRD Non-radiative decay

PBS Phosphate-buffered saline

PCB Printed circuit board

PET-G Polyethylene terephthalate glycol

RFU Relative reflective unit

SNR Signal-to-noise ratio

SPR Surface-plasmon resonance

TEM Transmission electron microscopy

t_{int} Integration time

TL Test line

TPU Thermoplastic polyurethane

TRF Time-resolved fluorescence

TSH Thyroid-stimulating hormone

UV Ultraviolet

Y Yttrium

Y_2O_3:Eu Europium-doped yttrium oxide

1. Introduction

The monitoring of biosignals in humans has been around almost as long as humans themselves. Over thousands of years measurement methods have changed from pure auscultation and visual inspection to the use of very specific and high-tech machines. Even simple instruments like the stethoscope have come a long way from a wooden cylinder to the models physicians are using today which contain a membrane to better pick up sounds of a certain frequency range and flexible tubes to enable the examiner to remain in a comfortable position [1].
First home-based diagnostic tools included clinical thermometers to measure body temperature during fevers. These instruments are another example of the development of diagnostics as they changed from using mercury to analyzing measurements based on infrared radiation detection within a few centuries.

Biosignals do not only differentiate in their way of measurement but also in their complexity. While simple signals like blood-pressure might be easily interpreted, more complex signals like the blood sugar level need more knowledge not only for their correct interpretation but also for the measurement process. As we currently know of an abundance of blood markers their analysis and co-interpretation gets more and more complex. Unfortunately, regular blood tests come with a lot of bureaucracy for patients which makes them less accessible. Even checking for values that might be of acute interest during diseases (e.g. CRP, C-reactive protein as a marker for inflammation) is not done sufficiently due to cumbersome processes.

The most famous at-home testing device is for sure the immunoassay pregnancy test. This rapid test uses urine as a sample and measures the amount of HCG (human chorionic gonadotropin), a pregnancy-related hormone. It was first developed in 1960 by Leif Wide and Carl Gemzell and first available to lay-users in 1977 [2]. Since then, test reaction times have decreased from several hours to a few minutes. The reason for the great success of this format is not only the demand but also the simple testing-flow and easy interpretation of results.

This shows that at-home testing devices have to be reliable, easy to use and cheap enough to guarantee a wide-spread usage.

1.1. Motivation

Diagnostics have universally found their way into our homes during the last years with Covid-19 antigen tests being present in almost every household. It is an important strategy to relieve healthcare personnel from simple tasks like regular check-ups for simple vitamin levels or the monitoring of the change of certain hormone levels to guarantee that even with the current lack of staff, crucial healthcare stays available. Home-testing devices which can not only test if an analyte is present in a sample but also in which quantity provide a solution for this problem and also decrease the amount of work and thought that is usually behind such check-ups, e.g. making an appointment at reasonable times, etc. This could further lower the resistance of patients to do regular tests which could in turn lead to earlier detection of abnormal values.

Most currently available home-testing systems which allow for quantitative analysis and are licensed for lay-use, use test strips based on gold nanoparticles (AuNPs). To ensure correct interpretation of results electronic readers are required. In the future, simple gold nanoparticle tests could be replaced by test strips using fluorescently-labeled markers and a corresponding reader. With this, an increase in sensitivity of up to several hundred times could be achieved [3, 4]. This is especially important for small analyte quantities.

Individualized healthcare is on the rise and the performance of self-tests is becoming a regular task for most people. With these changes to the traditional diagnostic timeline, new possibilities arise for manufacturers and development of new products is needed. Fluorescence-based immunoassays offer great potential as rapid self-testing devices as they are more sensitive while offering the easy testing flow that comes with lateral flow immunoassays, e.g. Covid-19 antigen tests. Together with an electronic reader, a broad test portfolio and personalized reports this technology could be the future in offering the best and simplest care possible.

The aim of this thesis is to further explore the usage of fluorescence-based lateral flow immunoassays (LFIAs) in a home-use scenario, with detailed research based on the Bloom (FLURE) Lab. This electronic reader is currently not capable of analyzing fluorescently labeled LFIAs but is compatible with a range of gold nanoparticle-based LFIA strips. Currently available tests monitor different blood marker levels, e.g. TSH, the thyroid-stimulating hormone which is a thyroid-specific marker, indicating possible over- or underfunction. The addition of fluorescence-based LFIAs to the test portfolio would allow for the expansion of detectable markers as this method offers lower limits of detection and will thus provide more sensitive tests. With this also analytes that can not be measured in a home-test scenario so far due to missing sensitivity of tests will be available and healthcare will become more easily accessible and personalized.

Different solutions for the read-out of LFIAs based on this reader are to be analyzed and improved, using material research, experiment conduction and analysis of results. It shall be ensured that any changes to the Bloom FLURE Lab do not interfere with the read-out of existing colorimetric, gold nanoparticle assays.

1.2. Lateral Flow Immunoassay

The intended measurement system is based on the principle of the lateral flow immunoassay. It is an analytical method to detect the presence or absence of a certain target analyte. Often referred to as a lab-in-a-hand, it has become one of the most well-known and most-used on-site test platforms in the modern world.

1.2.1. Working Principle

The term lateral flow immunoassay, as opposed to the more general term lateral flow assay, refers to the method of detection used in these devices. LFIAs use selective antibodies and antigens (thus the part “immuno”) as target-capturing entity, specific to the desired analyte. Depending on the working principle of LFIAs one can distinguish

between competitive and non-competitive assays, where the former method's test line intensity decreases with increasing analyte concentration and the latter shows a test line that increases in intensity with increasing analyte concentration. As non-competitive assays, also-called sandwich-type assays, are more commonly used this method shall be further described in the following paragraph.

Figure 1 shows the building blocks of a classical lateral flow immunoassay.

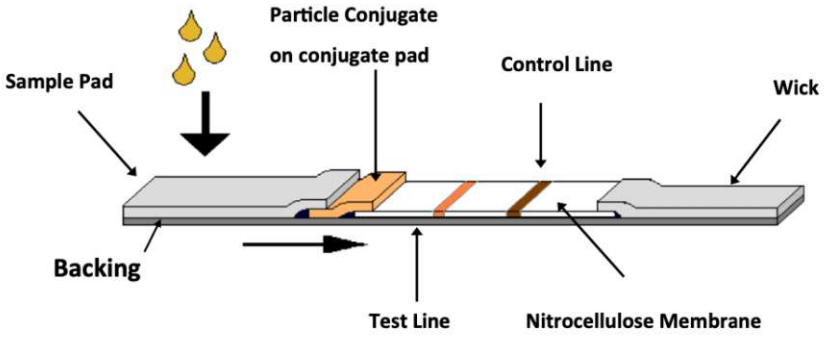

Figure 1: Components of a lateral flow immunoassay [5]

The sample pad is usually made out of cellulose or glass fiber and often carries reagents immobilized on the pad. The conjugate pad, generally made out of glass fiber or polyester, is the section where target-capturing antibodies first react with the analyte of interest. The next step in the flow process is a membrane made from cellulose nitrate, also called nitrocellulose membrane, which comes with two sections where test line antibodies and control line antibodies are immobilized, respectively. At the proximal end of the assay there is another cellulose or glass fiber pad, the so-called wick or absorbent pad, which guarantees that the sample will not flow backwards once it has traveled across the strip [6]. To guarantee correct positioning and contact between the different parts of an LFIA the test strip is mounted on a plastic backing. With this additional stability element correct sample flow is ensured.

Figure 2 shows a simple overview of the processes and reactions happening on the test strip. The individual steps taking place during the sample flow are explained in the following paragraphs.

The sample of choice (blood, serum, urine, saliva,...) is dispensed onto the sample pad whose porous structure allows for filtering of certain sample components, e.g. blood cells, clotting factors, etc. Due to capillary flow the sample then gets transported to the conjugate pad, where the antibody-label conjugates are immobilized. Upon sample flow reaching the conjugate pad, the dry conjugates get resuspended and the labeled capture antibody is able to bind to the target of interest, see fig. 2, top section.

Further on along the test strip another type of antibody is immobilized at the test line. When the sample, now holding label-antibody-target complexes, reaches the test line the target in this complex binds to the immobilized detection antibodies along the test line. It is "sandwiched" between the two antibodies, which is the reason why this type of LFIA is

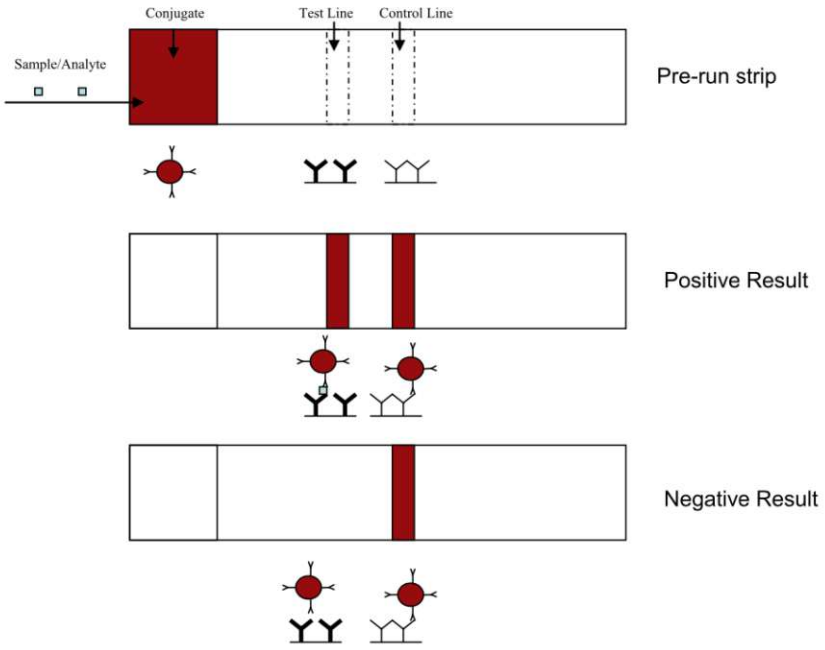

Figure 2: Working principle of a lateral flow immunoassay [5]

also called sandwich-assay, see fig. 2, middle section. If the target analyte is not present in the sample, the labeled capture antibodies can not bind to the secondary antibody on the test line and the test will give a negative result, meaning that no test line is visible, see fig. 2, bottom section.

Through accumulation of the labels along the test line it can not only be determined if the analyte of interest has been found in the sample but also the analyte concentration within the sample can be estimated or measured as it is directly linked to the line intensity. This can be done by comparing test line intensity with a given color grading system or with a calibrated reader, where the latter will give more accurate results. The control line consists of a different kind of antibody which is usually derived from an entirely different species and is there to catch any remaining labeled antibodies in the sample. It can thus be used as a control to guarantee that correct sample flow has happened. If this was not the case, no control line would be visible and the test can thus be discarded as invalid. This prevents the read-out of non-functional tests and with this the wrong interpretation of such tests.

The strips used for this thesis are further encased in a plastic test cassette leaving accessible only a small area for sample application on the sample pad and the read-out window, see fig. 3. Test cassette dimensions are 105×27×6 mm. On the inside of the test cassette another mechanism further ensures correct sample flow. Several well-aligned pressure points hold the test strip in place and increase contact between the different flow pads on the backing card.

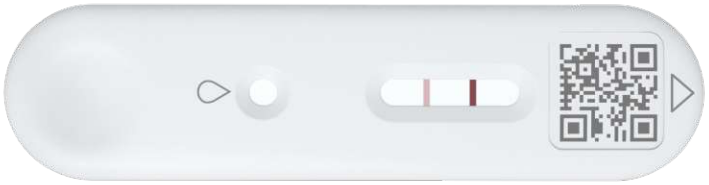

Figure 3: Bloom test cassette with visible test and control line; The QR code serves as identification marker of the test strip used by the reader. ©Bloom Diagnostics

The overall success of lateral flow immunoassays can be explained based on several of its properties: the so-called REASSURED criteria. This acronym summarizes all the important factors of an ideal point-of-care test and is explained in more detail below [6, 7].

REASSURED criteria:

1. **R**eal-time connectivity
2. **E**ase of specimen collection
3. **A**ffordable
4. **S**ensitive
5. **S**pecific
6. **U**ser-friendly
7. **R**apid and robust
8. **E**quipment free/Environmentally friendly
9. **D**eliverable to end-users

LFIAs fulfill all of the given criteria which explains their overall success, not only in medicine and diagnostics but also in other fields, e.g. food safety, veterinary, agriculture, industry, forensics and others [6, 8].

1.2.2. Quantitative LFIA Read-out

Quantitative read-out of lateral flow immunoassays is based on a calibration function, specific for each test. This function varies with different parameters of the test, e.g. maximal analyte adsorption concentration at the test line. This quantity can be altered by adjusting the parameters of any of the components used in an LFIA, e.g. membrane porosity. Also by adding detergent to the sample buffer and thus changing the sample's viscosity the sample flow velocity can be altered. A different flow speed results in a change in reactivity between capture and target molecules and thus a different maximal adsorption concentration which makes it necessary to use an individually adjusted calibration function

for every type of test strip. The same problem arises when analyzing the same strip with different readers. Reader specifications might be similar but not identical which calls for a specific calibration function for every combination of reader and strip.

Sensitivity of LFIAs can not only be altered by adjusting the test strip's components but is also defined by the label used to detect the analyte. Different labels have been reported in literature, e.g. AuNPs, cellulose nanobeads, latex nanoparticles, fluorescent labels, quantum dots, upconverting phosphors, chemiluminescent particles and magnetic nanoparticles [5, 9]. Each technique comes with its own advantages and disadvantages regarding sensitivity, synthesis, stability and ease of functionalization. Which particle is to be chosen for a test is highly dependent on the required sensitivity, assay stability in various conditions (e.g. high temperature), reproducibility and cost [5]. Read-out complexity also varies for the different particles and should be thus be considered in the choice of label.

While quantification needs additional equipment for all of the mentioned labels, some of them can be easily analyzed qualitatively with the naked eye, e.g. AuNPs, cellulose nanobeads and latex nanoparticles [5]. Simple qualitative read-out might be convenient in areas lacking higher infrastructure or for rapid diagnosis but when it comes to easy quantification, quantitative analysis by visual examination and comparison only is prone to faulty interpretation. For precise and reliable results electronic readers are required.

1.2.3. Gold Nanoparticle-based LFIAs

Colloidal gold nanoparticles are the most widely used labels for LFIAs.The first lateral flow immunoassay based on AuNPs was introduced in the 1980s, detecting a pregnancy-related hormone in urine [10]. The fact that this read-out mechanism is still preferred today is due to several properties of AuNPs [11, 12]:

- High physical and chemical stability
- Good biocompatibility
- Intrinsic bioaffinity allowing for easy and reliable surface modification
- Strong, robust signal

Colloidal AuNPs can be synthesized in different sizes, from a few nm to several hundreds of nm. Figure 4a shows TEM images of spherical AuNPs, with the right image revealing the narrow size distribution of the particles. Depending on the size the nanoparticles appear in different colors as can be seen in fig. 4b.

The AuNPs used for lateral flow assays usually have a diameter between 40 nm and 80 nm which makes them appear in dark red color, see fig. 4c.

It is necessary to use nanoparticles with small size distribution as this allows for an additional, more precise read-out mechanism than given by visual inspection alone. While qualitative read-out is facilitated by the red color of AuNP aggregates, quantitative measurements rely on a different method called surface plasmon resonance (SPR).

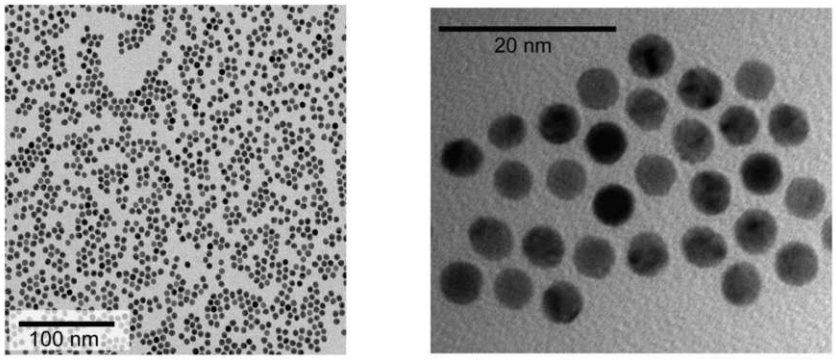

(a)

(b)

(c)

Figure 4: Gold nanoparticles: (a) TEM image of AuNPs of uniform size in two different scales [13], (b) Colors of monodispersed AuNPs of various sizes [14], (c) AuNPs in solution as used for LFIAs (image courtesy of DCN Diagnostics) [5]

Plasmons are quasi-particles describing a collective oscillation of free electrons in metal. They can only occur from photon-excitation at the metal surface and never in bulk material due to the dielectric properties of metals. In nanoparticles with a diameter much smaller than the wavelength of the exciting photon the induced oscillation will be distributed over the entire particle volume. In this special case the plasmon is referred to as localized surface plasmon. SPR is induced at a certain photon frequency or wavelength only, the so-called resonance frequency [15]. At this specific frequency, photon energy is absorbed and converted into an oscillation which leads to a decrease of reflected light. There are several

factors influencing the exact value of the surface plasmon resonance frequency of a metal, some of which are particle size, shape, composition and arrangement of nanoparticles [11]. Between gold nanoparticles with a diameter of 5 nm and 100 nm, the peak SPR wavelength shifts from 515 nm to 572 nm (green to yellow).

The 40 nm AuNPs that are used in many LFIA applications show maximal light attenuation at 525 nm which corresponds to visible green light, e.g. from an LED (see fig. 5).

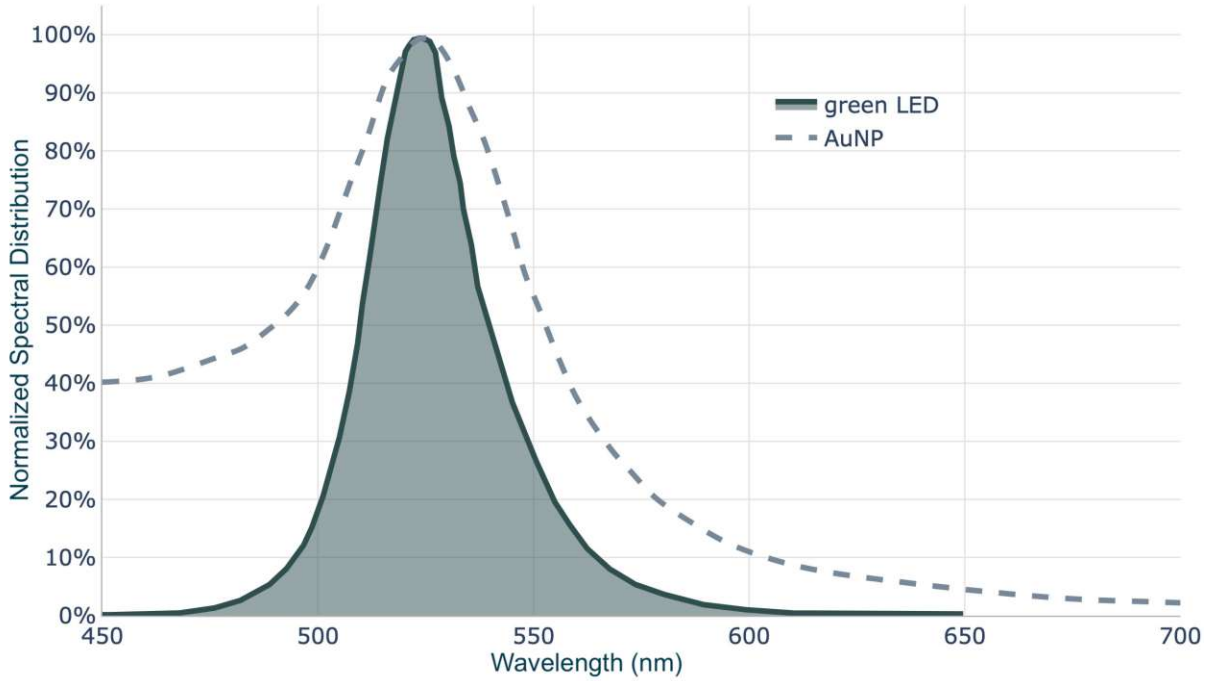

Figure 5: Emission spectrum of the green LED overlayed with the absorption spectrum of the AuNPs used [16]

Whereas the maximal absorption frequency is mostly material specific, the absolute absorption depends on the number of particles adsorbed at the test or control line and the extinction cross section of a single particle [17]. When using a green LED for LFIA illumination the test line will appear darker the more analyte is bound. The more colloidal AuNPs are available for SPR the more light gets absorbed and converted into oscillation which makes the analysis process relatively easy. With the measured total absorption and the calibration function that connects absorption to bound AuNP density, the analyte concentration in the sample can be calculated by the software of the electronic reader.

Disadvantages when using AuNPs in assays include their relatively low stability to changes in pH and salt concentration and the fact that their functionalization is limited to passive conjugation only [5]. This makes the use of AuNPs with undiluted samples difficult. Furthermore, due to their narrow size distribution these particles only appear in one color whereas other labels, e.g. cellulose nanobeads, can appear in multiple colors which makes visual read-out in an assay with several test lines easier. Cellulose nanobeads of different color are shown in fig. 6.

Figure 6: Cellulose nanobeads in solution (image courtesy of Asahi Kasei Fibers Corporation) [5]

Even though many LFIAs still rely on AuNPs their sensitivity is far below that of other reported technologies, e.g. fluorescent nanoparticles, where an increase in sensitivity of up to several 100-fold better than for AuNPs has been shown [3, 4]. For this reason, the feasibility of the implementation of fluorescent read-out of LFIA strips with the currently available electronic reader shall be investigated in this thesis. The principle of fluorescence will be explained in more detail in the following section.

1.3. Fluorescence

1.3.1. Principle

The emission of light upon relaxation of an excited electron is called luminescence. Depending on the spin states of the initial and excited molecule, luminescence can occur in two forms [18, 19]:

- Fluorescence: emission and conservation of the electron spin state of the atom
- Phosphorescence: emission and change in electron spin state of the atom

The electron spin state can be a singlet state, where the two electrons in an electron pair are spin-paired. This means that they both exhibit either spin up or spin down. The resulting spin has thus only one possible direction in space, which is why this state is called singlet state. The other option is a triplet state where one electron pair does not show paired spins, meaning they are either of spin up and down or down and up. This results is three possible orientations of the resulting spin state [19].

The processes of absorption, excitation and relaxation of electrons are best illustrated by a Jablonski diagram. Figure 7 shows such a diagram with the clear distinction of fluorescence (first excited singlet state S_1 to singlet ground state S_0) and phosphorescence (first excited triplet state T_1 to singlet ground state S_0).

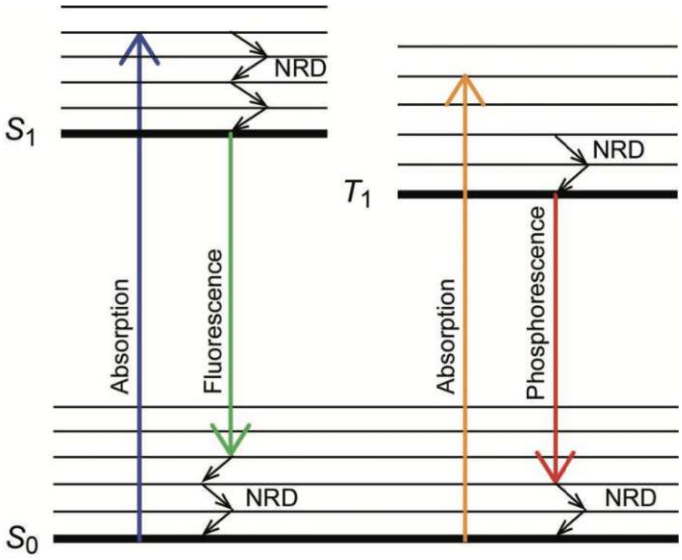

Figure 7: General Jablonksi diagram schematically showing the difference between fluorescence ($S_1 \rightarrow S_0$) and phosphorescence ($T_1 \rightarrow S_0$); Spin states are noted to the left of the depicted energy levels [20].

The wavelength of light that is able to excite an electron strongly depends on the internal structure of the molecule and its intrinsic energy levels. Due to the abundance of possible molecular structures this frequency can be quite broad in range. The emitted wavelength on the other hand has a narrow range. Electrons that get excited to different energy levels within the same spin states lose their excessive vibrational energy via non-radiative decay (NRD) until reaching the lowest energy level in their respective spin state [18]. This common energy level leads to a common relaxation of electrons after a fluorophore-specific life-time between picoseconds and hundreds of nanoseconds [19]. This relaxation corresponds to a narrow peak in the emission spectrum. Changes of the excitation wavelength will only result in a different intensity of the emission peak but not in a shift in the emission wavelength.

The difference between absorption and emission wavelength is called Stokes shift. A larger Stokes shift has several advantages, two of which are listed below [18].

- Easy differentiation between the two spectral peaks with the help of optical filters as they are not overlapping
- Reduction of quenching (intensity loss) through self-absorbance of emitted light by the fluorophore

Self-absorbance describes the re-absorption of radiation by the same sample that has emitted it. In fluorescence applications this effect happens only for molecules whose excitation peak spectrum and emission peak spectrum overlap. Self-absorbance leads to a reduction of the fluorescent signal as initial fluorescent emission already has lower energy than the initial excitation source (see fig. 7) and the lower the photon energy that is used for (secondary) excitation the lower the fluorescence intensity. The aforementioned

advantages lead to many applications preferring fluorophores with an intrinsic Stokes shift of several hundreds of nanometers.

1.3.2. Fluorophores

Some commonly used fluorescent labels are [5, 21, 22]:

- Organic dyes
- Metal-ligand complexes
- Fluorescent proteins
- Lanthanide complexes
- Semiconductor quantum dots
- Dye-doped polymer nanoparticles
- Fluorescent silica nanoparticles

The fluorophore-particles used during the practical experiments for this work are europium-chelate dyed nanobeads. Europium is a chemical element from the lanthanide family with atomic number 63. Lanthanides are generally also referred to as "rare-earth elements" and will form trivalent cations (Ln^{3+}). They exhibit long fluorescence life-times between 0.5 ms and 3 ms and a large Stokes shift. Europium-ions (Eu^{3+}) are the preferred label in many fluorescent assays as, out of all lanthanide-ions, they have the longest fluorescence life-time [23]. Peak emission wavelength of Eu^{3+}, lies at 612 nm which makes it appear bright red (see fig. 9). This wavelength is outside the range of classical background fluorescence by materials of the LFIA and biological samples which makes this fluorophore ideal for the use in immunoassays [5]. With the excitation wavelength and the emission wavelength not overlapping, quenching through self-absorbance is prevented and high fluorescence intensities can be achieved.

By chelation of Eu^{3+}-ions their fluorescent emission can be amplified. The chelate acts as a "collector" for the incoming exciting light by collecting energy and facilitates the subsequent energy transfer to the lanthanide ion. One example of a europium-chelate complex can be seen in fig. 8.

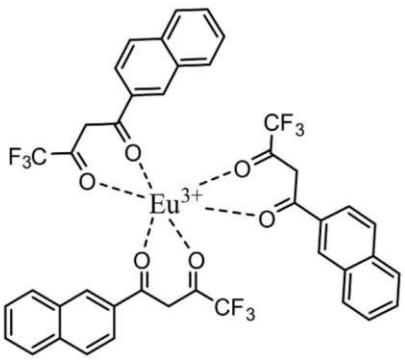

Figure 8: Example of a Eu^{3+}-chelate [24]

Upon chelation of the fluorescent element the excitation wavelength shifts and will correspond to the absorption spectrum of the chelate [23]. In contrast, the emission wavelength does not change as it is a direct function of the energy levels of the fluorescent ion. The emission and excitation spectrum of europium-chelate dyed nanobeads can be seen in fig. 9. By encapsulating the dye in polymer beads, leaking and unspecific binding of the fluorophore is prevented which helps to maximize the signal-to-noise ratio (SNR) [5].

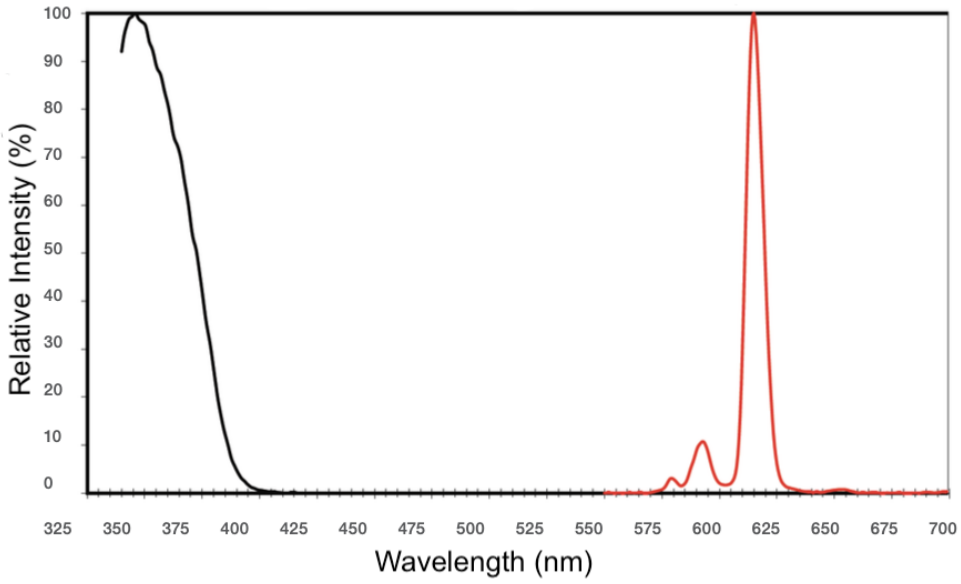

Figure 9: Excitation spectrum (black) and emission spectrum (red) of europium-chelate dyed polystyrene nanobeads [25]

1.3.3. Applications – Fluorescent LFIAs

Application of fluorescence is not limited to classical uses like fluorescence spectroscopy but has also found its way into the biomedical field in the recent years. Some examples are the use of fluorescent particles for diagnostics of neurodegenerative diseases and cancer and their use as labels in lateral flow assays [26, 27].

Fluorescent immunoassays mostly use detection antibodies functionalized with fluorophore-containing polystyrene beads. Upon binding of the antibodies along the test and control line and illumination of fluorophores, a fluorescent signal can be measured. The intensity of the signal will be directly correlated to the concentration of bound antibodies and thus analyte concentration.

Fluorescent labels show several advantages compared to the classically used gold nanoparticles [5]:

- Possibility of active conjugation allows for a variety of applications
- Higher sensitivity
- Availability of multiple colors allows for easy multi-parameter detection

Although fluorescence-based LFIAs come with many advantages this method of detection has to be chosen carefully as its labels also come with certain disadvantages [5, 18]:

- Machine-based read-out required
- Functionalization and stabilization can be difficult
- Less robust signal than other particles due to photobleaching
- Higher costs

Even though smaller analyte concentrations can be determined, the fact that fluorescent labels require machine-based read-out makes it impossible for fluorescence-based LFIAs to be used in low-infrastructure environments. The lower stability of fluorophores results in special storage conditions for fluorescent LFIAs (darkness, controlled temperature). Additionally, it is required to choose fluorescent labels carefully as they should exhibit a large enough Stokes shift and ideally, their emission wavelength should be outside of the spectral range of classical background fluorescent signals of biological samples or LFIA components. To optimize signal-to-noise ratio, autofluorescence of the sample and all other parts of the assay, e.g. membrane, test cassette, etc. has to be kept low which limits the choice of possible component materials. In an environment where storage conditions and the correct functioning of an electronic reader can be guaranteed, fluorescent nanoparticles offer great potential for the use in LFIAs.

1.3.4. Time-resolved Fluorescence

An additional option to maximize SNR in fluorescent applications is the use of time-resolved fluorescence (TRF). During a regular steady-state fluorescent read-out process images are captured while the sample is still illuminated by the UV source. This leads to high reflective noise and limits achievable contrast. This problem is solved using time-resolved fluorescence which exploits the typical fluorescent life-time of certain fluorophores, e.g. from the lanthanide family, reaching up to several hundreds of nanoseconds. In time-resolved fluorescent read-out processes fluorophores get excited by a light pulse shorter than the typical decay time of the excited state [19]. After the light pulse the only signal remaining is that of the fluorophores as any autofluorescence fades directly with the end of the light pulse. This allows for measurements without any noise by reflection or autofluorescent components (see fig. 10).

Time-resolved fluorescence comes with many advantages when it comes to fluorescence spectroscopy as it gives more information about the molecule of interest than the most commonly used steady-state fluorescence. These specific advantages are not relevant for the pure quantitative read-out of fluorescent LFIAs and shall thus not be further described in this chapter. Although time-resolved fluorescence might lead to better results in the read-out process, this solution could not be further analyzed in this work due to hardware and software restraints, but shall be considered for subsequent work. The complexity arises from the fact that the light pulse and the integration time of the sensor capturing the image have to be accurately timed in order to get useful results.

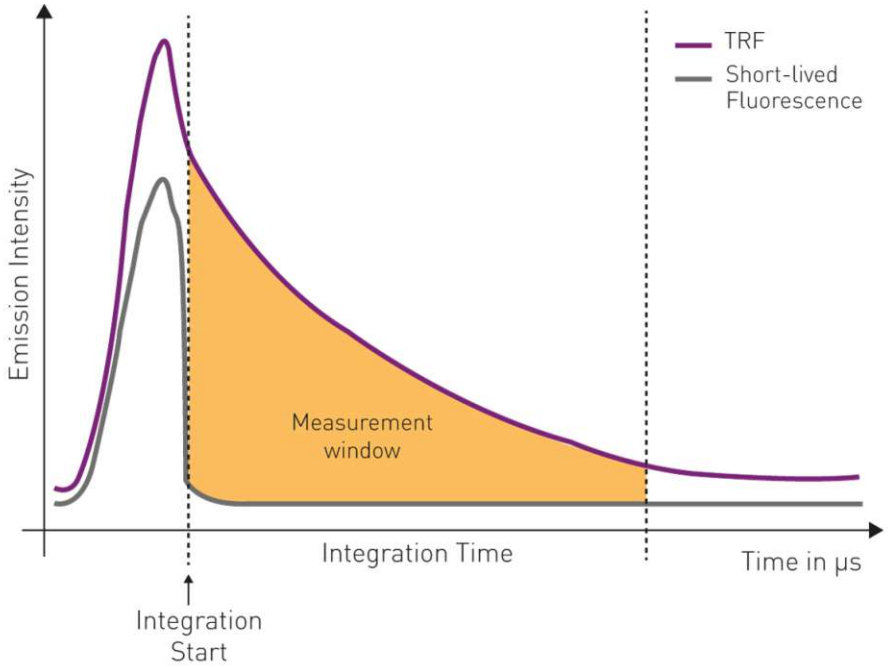

Figure 10: Principle of time-resolved fluorescence: after the light pulse (gray spike) and the correspondent fading of short-lived autofluorescence components, fluorescence measurement is conducted for a certain integration time. The yellow area under the curve gives the intensity of the measured signal [28].

1.3.5. Photo-degradation

Continuous UV illumination of Eu^{3+}-nanoparticles has been shown to lead to photobleaching of the fluorophore. Photobleaching or photochemical degradation describes a change to the molecule's internal structure and a resulting decrease of fluorescence intensity. The effect is highly sensitive to particle illumination time and light flux and also depends on the fluorophore itself, e.g. organic fluorophores degrade faster than inorganic fluorophores. The mechanism of photobleaching is based on reactive oxygen species which are generated by the interaction of the excited fluorophores and molecular oxygen. Another pathway for photodegradation, the oxygen-independent pathway, can be less easily described but seems to involve radical intermediates formed upon excitation and ionization of fluorophores in oxygen-depleted environments [29].

Experiments by Junger have shown that degradation of Eu^{3+}-nanoparticles on lateral flow membranes is increasing strongly with higher LED current while an increase of illumination time has less influence [16]. Further experiments by Junger revealed that degradation in the first few seconds of illumination can be approximated as a linear function, as can be seen in figure 11. Only after several tens of seconds of illumination the degradation function shows its exponential shape.

When introducing europium into a more stable host-matrix by doping another molecule, e.g. yttrium (Y), with Eu^{3+} increased photostability could be achieved, leading to more

reliable measurements [30]. Industrial uses of europium-doped yttrium oxide include dye-sensitized solar cells, luminescent sensors and LEDs [31].

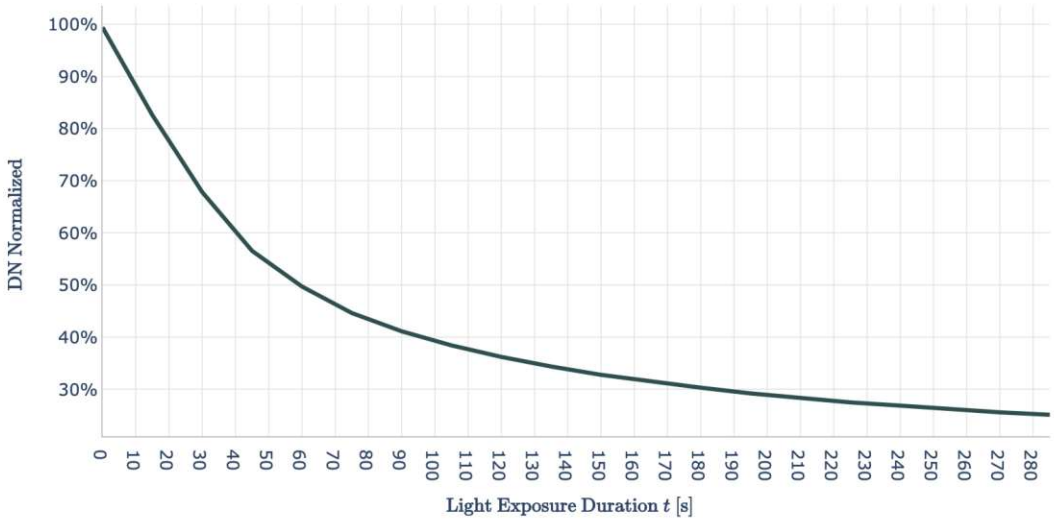

Figure 11: Degradation of fluorescence intensity as a function of the total illumination time, measured every 15 seconds; LED current = 500 mA, DN... digital number, derived directly from a CMOS sensor [16]

1.4. Bloom Lab

The Bloom Lab is a reader for colloidal gold nanoparticle-based LFIAs. Together with the Bloom Test and the Bloom App it forms the Bloom System (fig. 12) which supplies the user with personalized information about test results and suggested actions, e.g. dietary changes, doctor visit, etc.

Figure 12: The Bloom System comprising: a lateral flow immunoassay "Bloom Test" (left), the test platform "Bloom Lab" (middle) and the "Bloom App " for mobile phones (right); The Bloom Lab and the user's phone are connected via Bluetooth. ©Bloom Diagnostics

The analysis is based on six green LEDs (for more details see datasheet, fig. 42) with center wavelength of 525 nm. The placement and number of LEDs allow for uniform illumination of the test strip where the light gets partially absorbed by the AuNP labels along the test and control line due to surface plasmon resonance. The remaining light gets reflected and reaches the CMOS sensor (complementary metal-oxide-semiconductor sensor) which consists of 1280×960 active pixels (see datasheet, fig. 49). Each pixel comes with its own electronic circuit to directly convert incoming light to a corresponding voltage via the photoelectric effect, followed by amplification. The sensor thus measures the incoming light intensity for each pixel. As the Bloom Lab uses a monochromatic CMOS sensor for higher sensitivity, it is not possible to distinguish between different wavelengths once the image is captured. The overall light intensity within a certain, sensor-specific wavelength range reaching a pixel is converted into a value on the black-and-white scale in the final image, resulting in monochromatic images. From this information, the concentration of bound AuNP-labeled antibody-analyte complexes is calculated, as more light absorption and thus darker lines correspond to more AuNPs along the test line.

The use of a CMOS sensor brings several advantages compared to CCD cameras which are more regularly used to capture images of biological samples. All of these advantages are crucial for the application in home-based diagnostics:

- Good spatial resolution
- Small camera size
- Low energy consumption
- Low production cost

All main parts of the Bloom Lab can be seen in the side view section in fig. 13.
It consists of:

1. a CMOS sensor PCB
2. an objective which is placed inside the upper lightcone
3. a main PCB on which the LEDs are mounted
4. a lower lightcone
5. a test cassette inlet in which the cassette can be inserted from the outside through a small flap

An additional PCB can be seen on the left side of the Lab in fig. 13. This PCB does not have any computational power, it only helps the Bloom Lab “communicate” with the user via an LED light ring, showing booting status, connectivity, measurement status and possible error states.

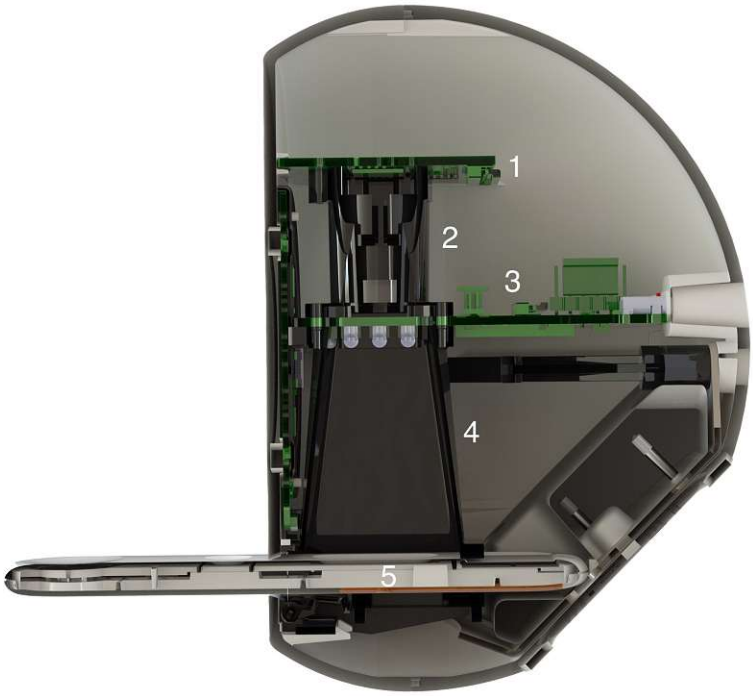

Figure 13: Inner side view of the Bloom Lab; CMOS sensor PCB (1), upper lightcone (2), main PCB (3) with LEDs, lower lightcone (4), test cassette inlet (5); total height = 121.6 mm

Bloom test cassettes are made from Acrylonitrile Butadiene Styrene (ABS), a polymer widely used in diagnostic applications also due to its excellent mechanical properties and its low melting-point allowing for it to be used in 3D-printed set-ups. As stated by Jurischka et al. in [32] ABS shows low autofluorescence compared to other plastics and is therefore considered suitable for fluorescence applications. This is important as test cassettes have no active purpose in the read-out process. Although they hold the test strip in place and guarantee correct sample application and sample flow the material itself should be as inactive as possible, e.g. regarding reflectance, autofluorescence, etc.

1.5. FLURE

As mentioned in section 1.4 the Bloom Lab currently uses LEDs emitting light in the green spectral range for the analyis of gold nanoparticle-based lateral flow assays. However, sensitivity of these assays is limited, as described in section 1.2.3. To further increase the Bloom Test portfolio and maximize achievable sensitivity, it is planned to use LFIAs with fluorescent labels in combination with the Bloom Lab in the future. For this, the hardware has to be adapted in order to being able to excite the chosen fluorophore and to detect the fluorescent signal. The development project was titled “FLURE”.

First steps into the FLURE project were taken from September 2021 to April 2022 [16]. Different setups were tested, including different kinds of sensors (CMOS, linear array and

spectral sensors) and different optical filters. The resulting prototype used a CMOS sensor for fluorescence detection and a longpass filter (LP475 from Edmund Optics) to improve SNR by filtering out unwanted autofluorescence signals or secondary LED peaks. The LEDs used in the final prototype of [16] are OSRAM LZ1-00UV0R UV-LEDs with a peak wavelength of 365 nm (see datasheet, fig. 43). Comparing this emission to the maximal absorption wavelength of europium-chelate dyed nanobeads (333 nm) fluorescence yield can potentially be improved by finding an LED of better spectral fit. Further possible improvements include a bandpass filter instead of the longpass filter to also account for optical noise in the UV range. LED currents of 200 mA and integration times of 20 ms were found to give the best results in [16] and shall therefore be used as a starting point in this thesis. As degradation of fluorophores seemed to be mostly influenced by LED power it is integration time that shall be further investigated to obtain an optimized SNR.

Further development of the FLURE project has been done for this thesis, including:

- Testing and comparison of different **UV-LEDs** for ideal spectral fit and illumination properties, e.g. viewing angle
- Improving the light path by investigating the correct **LED position** and the corresponding distance between LEDs and LFIA
- Further optimizing the light path by choosing an **optical filter** which allows for the read-out of the fluorescent signal and the signal generated with AuNPs
- Investigating the **autofluorescence of all materials** that are in the light path: test cassette, LFIA membrane, LFIA backing card and choice of a material combination which exhibits the lowest autofluorescence
- Increasing the SNR by adjustment of the integration time

For all of the mentioned steps, experiments were performed after extensive literature research only as this guaranteed high efficiency during the tests.

2. Materials and Methods

2.1. Test Set-ups

LEDs were tested for their ability to excite fluorescence of the chosen fluorophore and their optimal positioning with two set-ups: the "experimental unit" and the FLURE Prototypes.

2.1.1. Experimental Unit

The first set-up, called the "experimental unit", is an in-house-built wooden box with a lid to open it up completely. A disassembled Bloom Lab is located inside the box with 3D-printed stands and holders allowing for correct positioning of the relevant parts like the CMOS sensor, the objective, optical filters, LEDs and the LFIA strip (fig. 14).

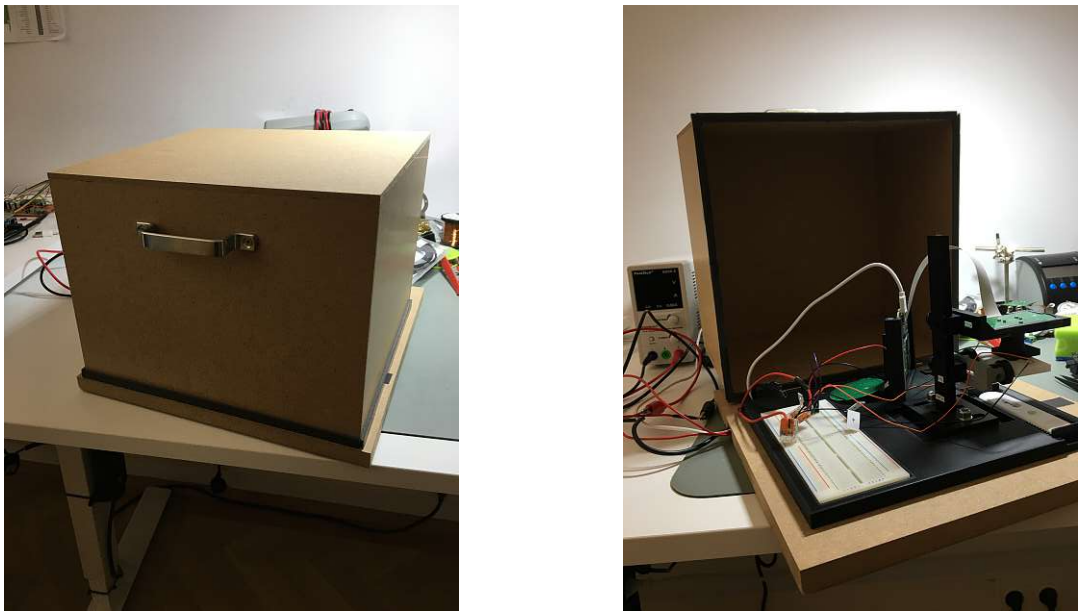

(a) exterior **(b)** interior

Figure 14: Experimental unit; dimensions with closed lid: 28×28×21 cm

The custom-made holders guarantee easy adjustment of the individual parts which allows for quick alterations of LED position and illumination angle. Two pairs of holders were designed from scratch in order to further simplify the test set-up. Figure 15 shows a rendered image of the newly designed, 3D-printed LED holders used to enable reproducible testing of surface-mounted device LEDs.

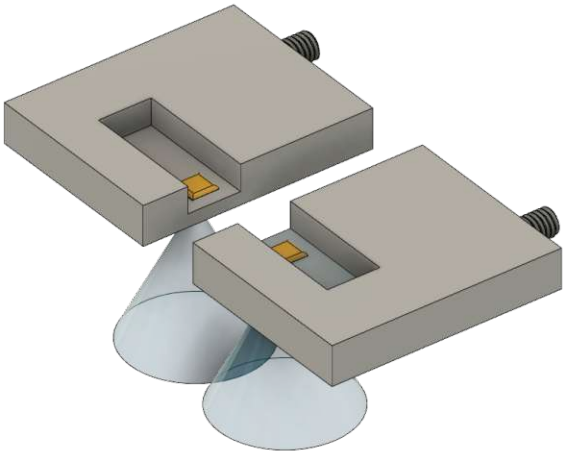

Figure 15: Two 3D-printed LED holders for easy testing of SMD LEDs, to be used symmetrically (see also fig. 16). LEDs are inserted into the square hole in order to illuminate the strip below (schematically shown with yellow shapes, light cones below). The elongated indentations allow enough space for the cables soldered to the LEDs' electrodes. The threads are used to adjust the illumination angle and to connect the 3D-printed holders to the already available stand of the experimental unit. Dimensions of one holder are 35×28×6 mm without the 3D-printed thread.

The experimental unit shall be used to investigate the influence of LED position, whether placing the UV-LEDs on the main PCB or inside the lower lightcone is favorable. For this it is necessary to mimic these different positions, regarding LED-LFIA distance and illumination angle. The relevant parameters were measured from a regular Bloom Lab and transferred to the experimental unit.

LED-LFIA distance was measured to be 4.5 cm for PCB position and 1.9 cm for lightcone position. The illumination angle in lightcone position is 35°.

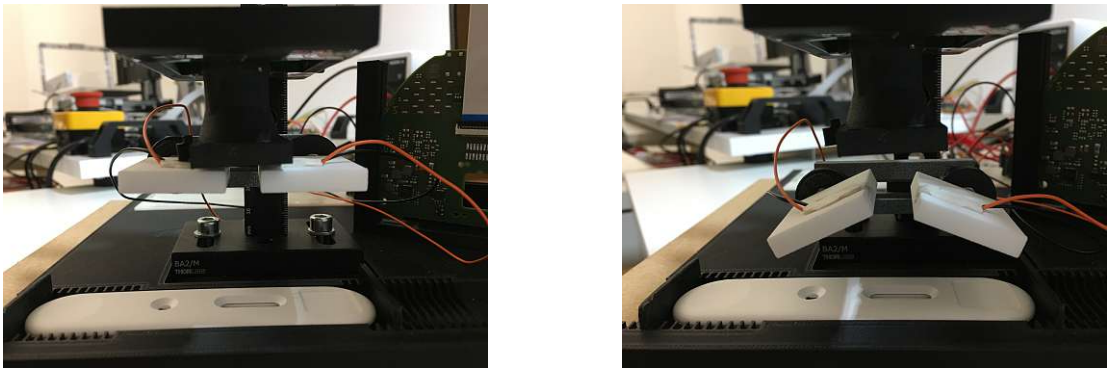

(a) PCB position **(b)** LC position

Figure 16: PCB and lightcone position as mimicked in the experimental unit; UV-LEDs are placed in the two symmetrically positioned holders (white), 3D-printed according to fig. 15.

Voltage supply for the experimental unit is external and can thus be set to any value. This offers the possibility of testing LEDs independently of the Bloom Lab hardware.

2.1.2. Prototypes

To test the performance of UV-LEDs in a more realistic setup three prototypes were produced by Bloom's manufacturing partner Cicor (Cicor Management AG, Switzerland). All of the prototypes have built-in UV-LEDs whose position cannot be changed which makes more consistent measurements possible than can be performed with the experimental unit. Every prototype was built to investigate a different UV-LED model but also the position of the LEDs changes. For Prototypes 1 and 2 the UV-LEDs are placed in the lower lightcone, which corresponds to the already mentioned lightcone position. Prototype 3 has its UV-LEDs soldered onto the main PCB, also referred to as PCB position.

For the production of the prototypes, regular Bloom Labs with six green LEDs were altered and customized in order to investigate different combinations of parameters in the actual setting of a Bloom Lab. The prototypes also still include green LEDs as future versions of the Bloom Lab are required to read out both types of lateral flow assays, fluorescence- and AuNP-based. A summary of the properties of the three prototypes is listed below.

- **Prototype 1**
  - 6 green LEDs: OSRAM LT T64G
  - 2 UV-LEDs: OSRAM LZ1-00UV0R
  - UV-LED position: lower lightcone, see fig. 17
- **Prototype 2**
  - 6 green LEDs: OSRAM LT T64G
  - 2 UV-LEDs: Luminus SST-10-UV
  - UV-LED position: lower lightcone, see fig. 17
- **Prototype 3**
  - 4 green LEDs: OSRAM LT T64G
  - 2 UV-LEDs: Broadcom Inc. AUV3-SQ32-0RT0K
  - UV-LED position: replacing two green LEDs on the main PCB (position similar as can be seen in fig. 13)

The UV-LEDs in Prototype 1 and 2 have to be powered externally as it was not possible to install direct cables from the main PCB of the Bloom Lab to the LEDs in the lower lightcone. The lightcone had to be modified to fit the UV-LEDs and was designed to have angular shape. The outlines of the adapted lower lightcone and the connectors used to power the UV-LEDs can be seen in fig. 17. For Prototype 3 direct powering through the power supply of the Bloom Lab was possible as the UV-LEDs were soldered onto the PCB, replacing two green LEDs.

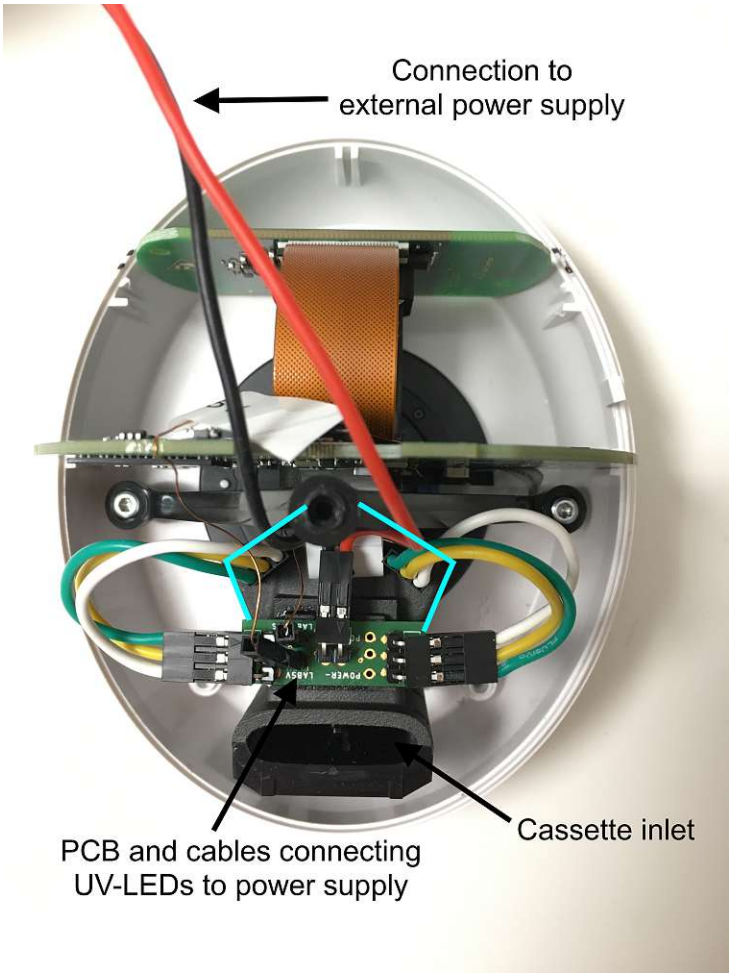

Figure 17: Interior of Prototype 2; Light-blue lines show the outer shape of the modified, angular lower lightcone allowing for integration of UV-LEDs. The extra PCB allows for the activation of the UV-LEDs with the Bloom Lab's software.

In [16], Prototype 1 and 2 were already investigated. It was found that SNR was up to 40% higher in Prototype 1 compared to Prototype 2. This is most likely due to the OSRAM LEDs exhibiting smaller viewing angle than the Luminus LEDs (OSRAM: 64°, Luminus: 130°). This leads to a more focused light exposure of fluorophores and thus higher fluorescence yield in Prototype 1 which was therefore deemed the more suitable set-up out of the two prototypes [16].

Prototype 3 was built in the course of this thesis after extensive literature research regarding the optical properties and illumination parameters of LEDs. Broadcom LEDs show a similar peak emission wavelength (365 nm) but a smaller viewing angle (35°) than OSRAM UV-LEDs. Additionally, placement of the UV-LEDs changes from Prototype 1 (lightcone position) to Prototype 3 (PCB position). As it was not clear, how these alterations to the LED's parameters and the lightpath affect the performance of the prototypes a direct experimental comparison between the two versions is necessary.

2.2. UV-LEDs

This section focuses on the different UV-LED models that were tested for their suitability of implementation in the Bloom FLURE Lab. Primary research for LED models was performed online. This comprised the scouting for LEDs in multiple manufacturer's databases, reaching out to the individual suppliers to obtain an offer and finally deciding on the LED models that should be tested for this thesis.
Requirements UV-LEDs have to fulfill in order to be included in the experiments are listed below:

- Suitable peak wavelength for the excitation of Eu^{3+}-NPs
- LED size $< 4.5 \times 4.5$ mm to enable implementation of the LED on the main PCB
- Forward voltage < 4V as this voltage can be supplied by the PCB without changes to the internal electronics of the Bloom Lab
- Not too expensive, meaning in direct comparison of two similar LEDs the less expensive one was chosen

Experiments were planned to compare new LED models as well as LED models that had already been investigated in the past. After the performed online research, five LED models showed promising parameters and were decided to be included in the tests. Figure 18 shows the selected LEDs, table 1 gives an overview of their specifications. LED models shall further be referenced by their individual supplier's name as this allows for a more easily readable format.

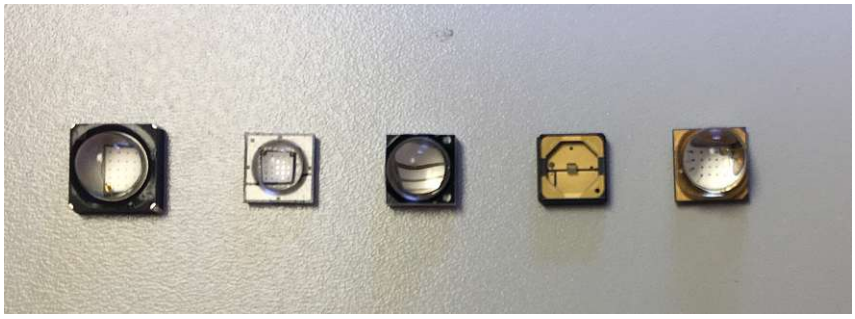

(a) top view

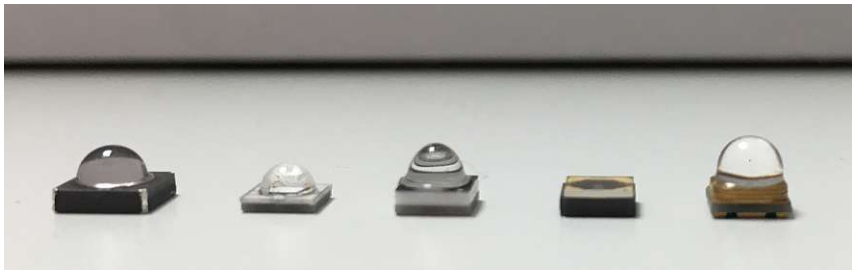

(b) side view

Figure 18: Tested UV-LEDs, from left to right by supplier: OSRAM, Luminus, Broadcom, Neumüller, IBT; LED footprints are between 3.5×3.5 mm and 4.4×4.4 mm for all models.

Name	Supplier	$\lambda_{peak} \pm \Delta\lambda_{1/2}$ (nm)	Angle (°)	U_f [I_f] (V [mA])
LZ1-00UV0R	OSRAM	365 ± 12	64	3.4 [100]
SST-10-UV	Luminus	365 ± 10	130	3.4 [100]
AUV3-SQ32-0RT0K	Broadcom Inc.	365 ± 11	35	3.7 [100]
CUD1GF1A	Neumüller	310 ± 11	120	6.2 [20]
IBT-L3535-UV	IBT	340 ± 14	60	4.4 [100]

Table 1: Overview of tested LEDs showing the article name, supplier, peak wavelength and peak width at 50% intensity (FWHM), viewing angle, and needed forward voltage U_f for the given forward current I_f as stated in the individual datasheets (Appendix fig. 43-47).

Previous experiments by Junger focused on LEDs with a peak wavelength of 365 nm which is higher than the mentioned 333 nm excitation wavelength of europium-chelate nanobeads [16]. As excitation capability of UV light depends on its photon energy, it was suggested that wavelengths that are below the excitation wavelength and thus higher in energy might lead to more efficient excitation than wavelengths that are above the excitation wavelength. This theory was tested by including one UV-LED model with a peak wavelength of 310 nm (Neumüller). Another LED model that was tested has a peak wavelength of 340 nm (IBT) which is expected to provide the best spectral fit for the excitation of Eu^{3+}-nanoparticles. The three LEDs with peak wavelength 365 nm (OSRAM, Luminus, Broadcom) exhibit different viewing angles and thus a differently focused illumination (see table 1).

As can also be seen in table 1, Neumüller and IBT models need higher forward voltage than can currently be supplied by the main PCB of the Bloom Lab (4V). Nevertheless, it was decided that they should still be considered for testing due to their peak wavelengths being different than that of any LED tested before. If measurements show an above-average improvement of fluorescence yield Bloom FLURE Lab components might be altered in order to allow for these LEDs to be used.

2.3. Optical Filter

As described in [16], optical filters are needed to cut off unwanted wavelengths and obtain a valuable image for analysis with the Bloom FLURE Lab. This theory was also tested with Prototype 3 and longpass filters by Schott (GG475 in the prototype and LP475 in the experimental unit) were then used in all following experiments. Both filters show the same characteristics with a cut-on wavelength of 475 nm but the product name changed between orders which is why both labels occur in the text.

Filter diameter was 12.5 mm for both applications but thickness changed from 1 mm in the prototype to 3 mm in the experimental unit, due to different mounting options. With application of one of these filters noise by UV illumination is not only minimized but they also allow for transmission of the signal used for AuNP-based read-out (525 nm).

This feature enables a combination of both read-out mechanisms in one reader for future experiments. Filters appear yellow (see fig. 19) and were mounted directly on the objective facing the test strip for all experiments.

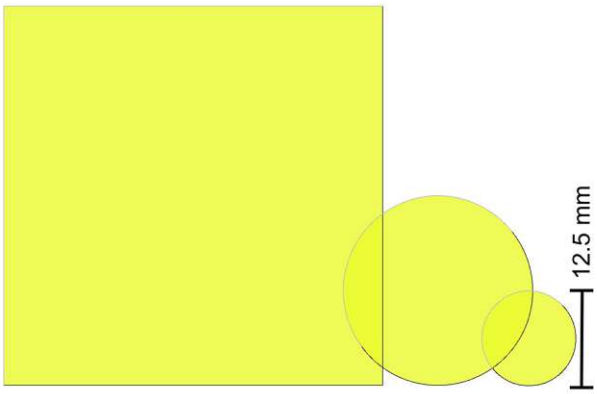

Figure 19: GG475 longpass filter by Schott in different sizes [33]; The filter appears yellow. For datasheet see Appendix fig. 48

2.4. LFIA Membrane

Seven different combinations of membranes and backing cards were tested for their autofluorescent properties. The membranes show similar composition, as they are all made of cellulose nitrate, but differ in effective flow speed due to their pore sizes. The flow speed of an individual membrane type can be read from its product name. The first letters (CN, FF, HF) give information about the supplier producing the membrane. The numbers following the letters are the time in seconds that it takes for a front of distilled water to rise 4 cm along the membrane when one end is inserted into a pool of water. Nitrocellulose membranes ending with smaller numbers exhibit faster flow due to larger pore size, while large numbers indicate smaller pores.

Tested membranes are shown in fig. 20. It is impossible to distinguish between the different membranes with the naked eye which makes careful handling and labeling necessary to allow for reliable results. The tested combinations of membrane and backing card shall be referred to with the abbreviations below:

- CN95 (Sartorius), with transparent backing
- CN140 (Sartorius), no backing
- CN150 (Sartorius), with white backing: CN150W
- CN150 (Sartorius), with transparent backing: CN150T
- FF80 (Cytiva)
- FF120 (Cytiva)
- HF120 (Millipore)

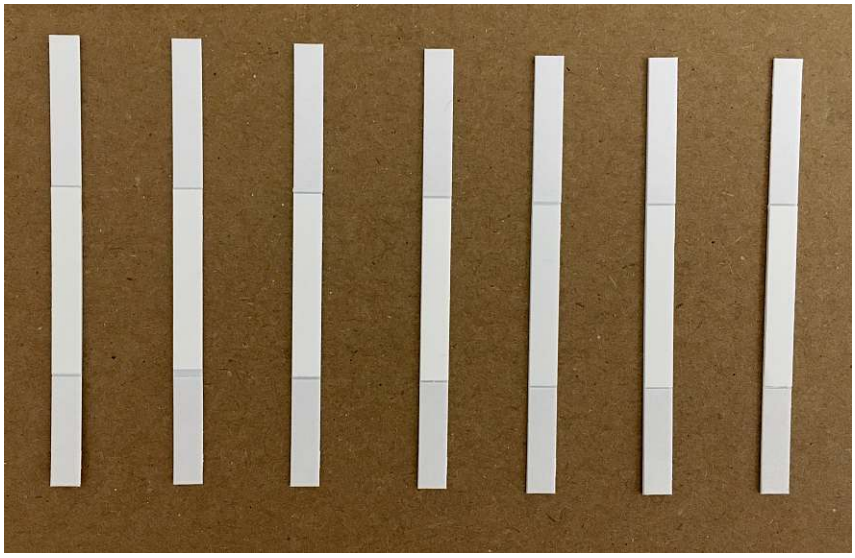

Figure 20: Tested lateral flow membranes, from left to right: CN95, CN140, CN150W, CN150T, FF80, FF120, HF120; dimensions: 60×4 mm

All tested membranes consist of cellulose nitrate which is classically used for lateral flow assays. The differences in pore size and the different backings could not only alter autofluorescent but also reflective properties and could thus influence SNR due to increased background noise. For fluorescence assays, it is recommended by Sartorius to use cellulose nitrate membranes on white backing. It is unclear if the backing card itself affects the fluorescent read-out signal which makes experiments on the influence of this property necessary.

Membranes were tested with Prototype 3. Experiments included a direct comparison regarding membrane autofluorescence and reflectance in dry and wet state, using MilliQ water.

2.5. Cassette Material

As stated in section 1, Bloom test cassettes are made from ABS which shows low autofluorescence compared to other plastics, like PET-G (polyethylene terephthalate glycol) and TPU (thermoplastic polyurethane) [32]. However, the white surface of the cassette is also visible inside the reading window and leads to a certain level of background due to light being reflected off the surface. To find the best cassette material for fluorescent applications of the Bloom Lab three different cassettes were evaluated (see fig. 21):

- white ABS: newest test cassette used by Bloom
- black ABS: white ABS test cassette, sprayed with black UV-resistant lacquer with matte finish
- white Makrolon: robust, lightweight, white polycarbonate cassette used for earlier Bloom tests

Figure 21: Tested cassettes, from left to right: white ABS, black ABS, white Makrolon; dimensions in assembled state: 105×27×6 mm

It is likely that black spray paint does not exhibit the same properties as actual black ABS test cassettes. Nevertheless, it was deemed sufficient for testing the influence of cassette color on the read-out, as actual black ABS was not available for this thesis.

Cassette autofluorescence was evaluated using Prototype 3. Images of fluorescent reference strips were captured and evaluated in regards to the ratio of the mean-gray value (MGV) of the test line and background to investigate the influence of the cassette material on the read-out process.

2.6. Fluorophore Testing

Europium-doped yttrium oxide (Y_2O_3:Eu) was purchased from Merck KGaA. The product website specifies the excitation wavelength at 254 nm [34]. Due to its higher optical stability and decreased fluoro-degradation when comparing it to regular Eu^{3+}-NPs this rare earth-doped metal oxide was to be used in all experiments to determine most suitable LED model and position without having to mathematically compensate for any degradation losses during analysis. Performed steps included dissolution of Y_2O_3:Eu, measuring fluorescent properties with a spectrofluorometer (Tecan Spark10M Multi Mode Microplate Reader), dispersion of the solution onto LFIA membranes and measurement of the resulting fluorescent signal with Prototype 3.

Before carrying out any experiments analyzing the prototypes' fluorescent read-out capability and the influence of possible components, the suitability of Y_2O_3:Eu as a fluorophore had to be assessed in separate experiments. Only after analysis of these initial tests were actual experiments regarding the choice of LED model and position performed with this fluorophore.

The compatibility of Bloom's FLURE Lab with regular fluorescent LFIAs on the market was investigated using Prototype 3 and test strips for quantitative measurement of TSH in serum by AllTest.

2.7. Data Analysis

Measurements assessing the ability of a setup to excite the fluorophore used were done using fluorescence standard strips. Different fluorophore concentrations were used to achieve various signal intensities, to investigate the possible fluorescence measurement range. Fluorophore density ranged from 1 ng/cm up to 250 ng/cm. The reference test strips were purchased from Senova (Senova Immunoassay Systems, Germany), a development partner company specialized in lateral flow assays. The given unit of ng/cm is the unit most commonly used for fluorescence assays and shall thus also be used within the scope of this thesis.
Fluorescence performance of reference strips was tested with the ESEQuant LR3 fluorescence reader (Qiagen) by the supplier. This laboratory-grade reader can distinguish between different fluorophore concentrations as low as 1 ng/cm. By measuring all of the different reference strips with the FLURE Lab it can be determined if this prototype allows for the read-out of signals across this range.

During an experiment the Bloom Lab activates the UV-LEDs and simultaneously captures an image of the test strip with its built-in CMOS sensor. Image parameters like the integration time can be preset and were adjusted for every measurement to guarantee ideal SNR. To avoid any influence from previous experiments and investigate repeatability, measurements were repeated for up to nine times for every setting. The images were then further processed and evaluated with ImageJ. Data analysis steps are listed below:

1. Choosing a region of interest around the test line (TL) or control line (CL) and a corresponding region in the background (BG)
2. Automatic calculation of the MGV, resulting in information about the fluorescence yield
3. Applying degradation correction using a linear correction function (according to [16])
4. Averaging of values of repeating measurements
5. Dividing TL or CL MGVs by the corresponding background value to get background-corrected MGVs
6. Plotting of the resulting TL/BG or CL/BG values and comparison of individual results

Analyis workflow is further visualized in fig. 22.

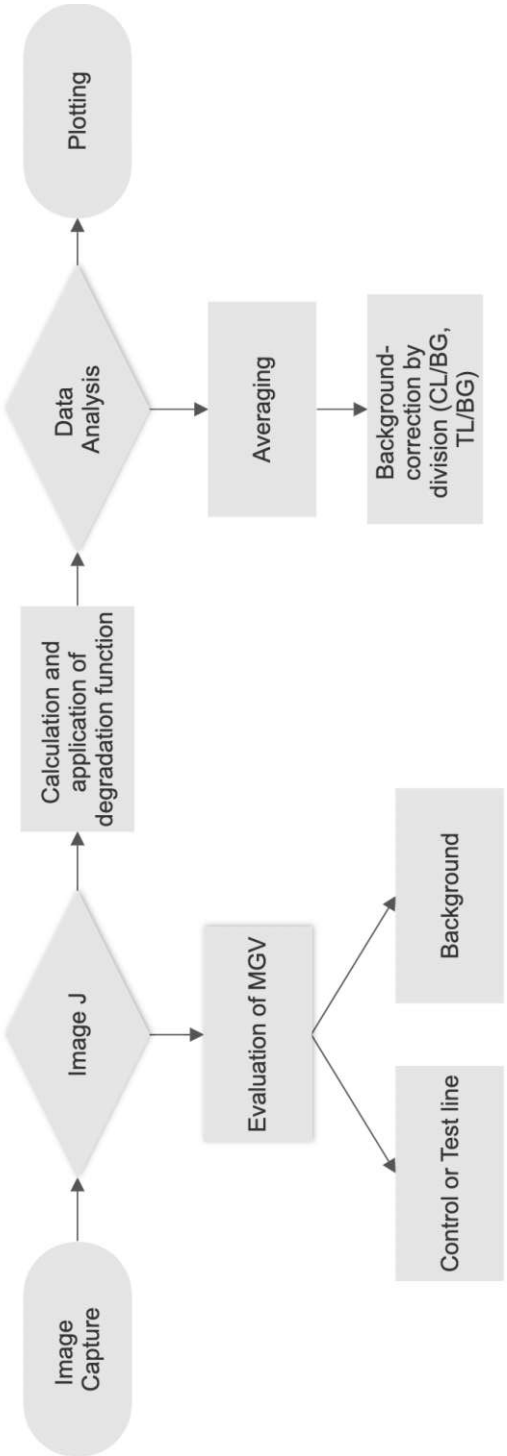

Figure 22: Workflow for analysis of experiments

3. Results and Discussion

This chapter summarizes the findings of the performed experiments. It is divided into several subsections, each focusing on one specific part of the future FLURE setup.

3.1. Optical Filter

As CMOS sensors are not typically used in UV applications, it is possible that the normal sensor objective is not enough to filter out unwanted reflection from the illumination of the test strip with UV light. This section shows the results of experiments done with Prototype 3, whether an optical filter would be necessary when using the in-built Broadcom LEDs.

For this a nitrocellulose membrane without fluorescent properties (CN150T) encased in a Bloom test cassette was inserted into the prototype. An image of this membrane was then taken in dry state with different integration times. At 10 ms the membrane showed such high reflection that the image was saturated, meaning no actual image analysis could be done (fig. 23).

Figure 23: Bare membrane, image taken without filter; $t_{int} = 10$ ms, cassette used = ABSW

10 ms are on the lower range of integration times needed to obtain a reasonable fluorescent signal as lower integration times would not allow for enough light to reach the sensor. Weak signals might even need higher integration times which is not possible without the use of an optical filter as the CMOS sensor is too light-sensitive for wavelengths in the UV range.

An optical longpass filter by Schott (GG475) was mounted to the objective in Prototype 3 and a test strip with a fluorophore density of 250 ng/cm was inserted. Images of this test line were then taken and evaluated (fig. 24). An integration time of 10 ms was found to be the minimum time needed to be able to analyze the image.

Figure 24: Reference membrane, image taken with optical longpass filter GG475; t_{int} = 10 ms, cassette used = ABSW

Test lines with a fluorophore density as low as 1 ng/cm could still be evaluated with Prototype 3 when using an integration time of 50-100 ms (fig. 25). Integration times this high would only result in a saturated image without any optical filter. In order to obtain similar results to a laboratory-grade fluorescent reader (as used by Senova in the classification of reference strips, see section 2.2) this optical component is crucial for the functionality of the Bloom FLURE Lab.

(a) t_{int} = 10 ms

(b) t_{int} = 20 ms

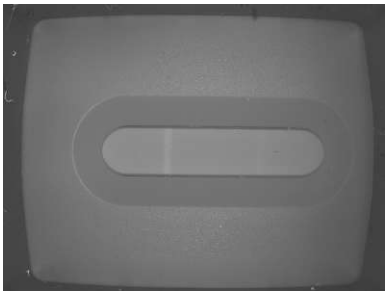

(c) t_{int} = 50 ms

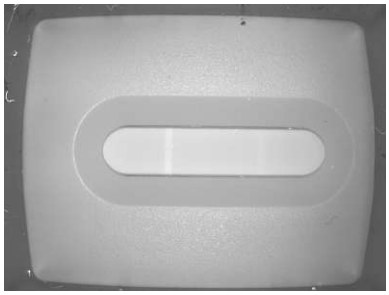

(d) t_{int} = 100 ms

Figure 25: Images taken with Prototype 3 and longpass filter GG475 (Schott); Fluorophore density is 5 ng/cm and 1 ng/cm for left and right testline, respectively. Integration times ranging from 10 to 100 ms, cassette used = ABSW

3.2. UV-LEDs

Five different UV-LED models were tested in this section. First, experiments were performed to assess each model's capability to excite fluorescence. Secondly, different LED placements within the FLURE Lab were investigated as these positions were mimicked in the experimental unit. Finally, additional experiments were done to ensure feasibility of the combination of fluorescence- and gold nanoparticle-based assays in one reader.

3.2.1. Type of UV-LED

All mentioned LEDs (Table 1) were tested with the experimental unit at an LED-LFIA distance of 4.5 cm and an illumination angle of 0°, corresponding to the regular distance and angle between the main PCB and the test strip inside the Bloom Lab.

Figure 26 shows the results of a first direct comparison. Voltage was set to 4V for all LEDs, except for the LED model by Neumüller which used 6.2V according to the datasheet. Forward voltage was also the same for all LEDs (100 mA), again excluding the Neumüller model, using 20 mA. Even though parameters were adjusted according to the datasheets to ensure proper functioning of the LEDs the differences in fluorescence yield are clearly visible.

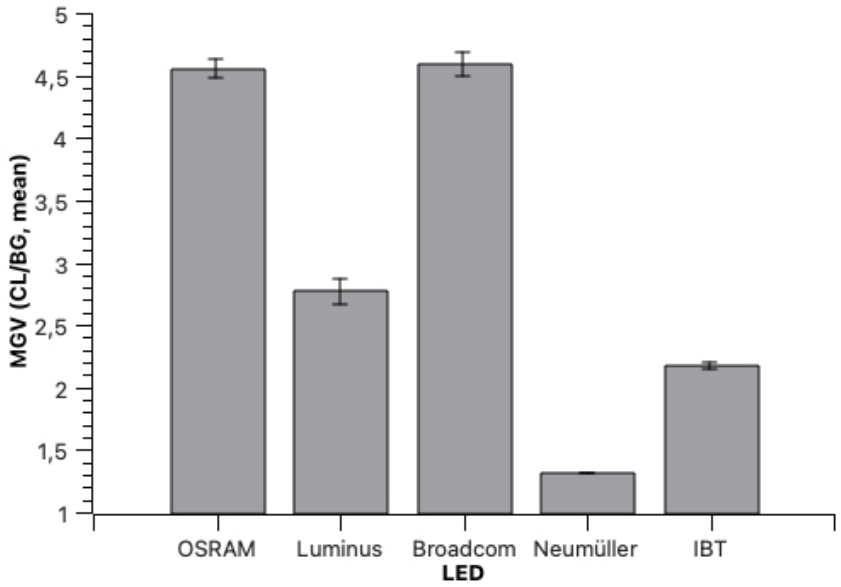

Figure 26: Results of different LEDs in PCB position; $t_{int} = 100$ ms, cassette used = ABSW; Error bars correspond to one standard deviation, calculated over three repetitions done for each setting.

LED models from OSRAM and Broadcom seem to show almost the same efficiency in exciting fluorophores. IBT and Luminus models result in a lower MGV but still allow for a fluorescence signal to be detected. The images taken while using the LED by Neumüller were almost completely dark and the fluorescent control line used for evaluation of this experiment could not be distinguished from the background although integration time was

set to 100 ms. The long integration time led to saturation of the signal acquired with OSRAM and Broadcom models which shows the strong difference in suitability of LEDs for this application.

Although the excitation wavelength of europium-chelate dyed nanobeads is stated to start at 333 nm in the nanoparticles' datasheet the two best LEDs show a peak wavelength of 365 nm. Even with the given peak width of 365 ± 12 nm and 365 ± 11 nm for OSRAM and Broadcom models, respectively, it is not fully clear as to why these models perform so well compared to theoretically better fitting wavelengths (e.g. IBT model, 340 nm).

The saturated signal prevents a detailed comparison between the two leading LED types and required thus a follow-up experiment.
An experiment comparing the OSRAM and Broadcom models at 25 ms integration time found similar results as the initial experiment, with a 8% higher fluorescence signal for the Broadcom LED (fig. 27). This proves that even though 100 ms of integration time led to signal saturation and thus a loss of signal, enough information was available to compare the two LEDs. The relative performance of the LEDs seems to be unaffected by the changed integration time. This information is valuable not only for future experiments but also when it comes to deciding on the LED model to be used for future Bloom FLURE Labs.

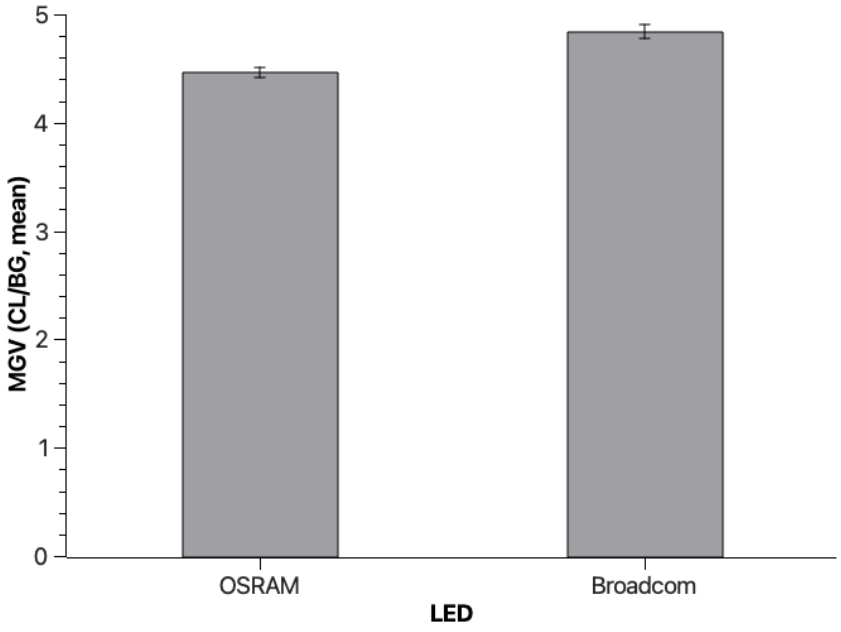

Figure 27: Detailed comparison of OSRAM and Broadcom LEDs in PCB position; t_{int} = 25 ms, cassette used = ABSW; Error bars correspond to one standard deviation, calculated over nine repetitions done for each setting.

3.2.2. LED Position

After the first results, OSRAM and Broadcom LEDs were compared at lightcone position with an LED-LFIA distance of 1.9 cm and an illumination angle of 35°. The initial

integration time of 25 ms led to signal saturation in images taken with the model by Broadcom. The experiment was thus repeated with a decreased integration time of 10 ms. Using these parameters, Broadcom models resulted in a 16% higher fluorescent yield compared to OSRAM LEDs.

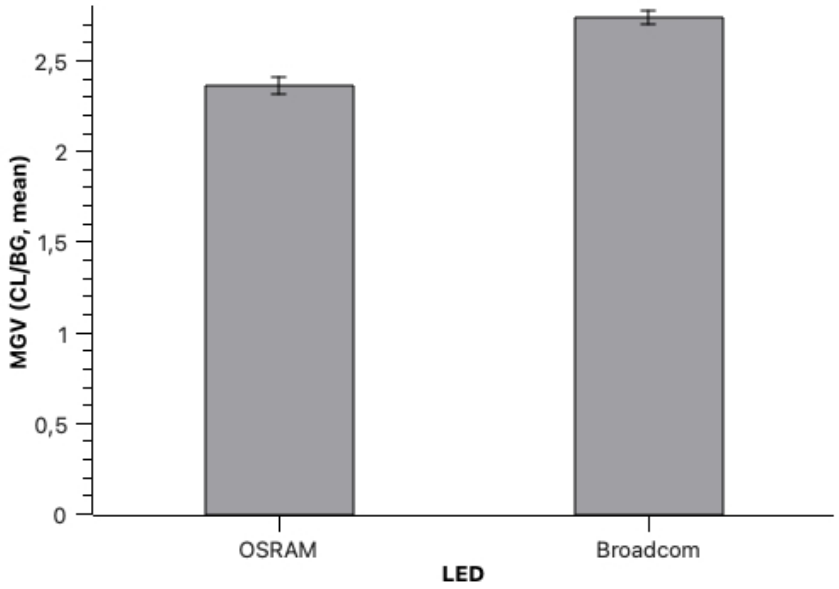

Figure 28: Detailed comparison of OSRAM and Broadcom LEDs in lightcone position; t_{int} = 10 ms, cassette used = ABSW; Error bars correspond to one standard deviation, calculated over nine repetitions done for each setting.

Differences in fluorescence yield between LED models with the same peak wavelength are most likely due to differences in the LED's viewing angle with the LED with the largest angle (Luminus, 130°) resulting in the lowest MGV and the LED with the smallest viewing angle (Broadcom, 35°) resulting in the highest MGV. Similar results obtained in experiments with the prototypes support this conclusion (see section 3.2.4).

Another factor could be differences in secondary emission peaks of the LEDs which lead to illumination in unwanted regions of the light spectrum. Unfortunately, these peaks are not specifically mentioned in the LEDs' datasheets which allows no closer investigation into this topic in this thesis. The theory of the influence of secondary peaks could be tested in future work upon usage of an LED emission filter allowing only for light in the desired UV range to reach the LFIA.

As the LED model by Broadcom showed high to highest fluorescence yield in all experiments, this model was chosen to conduct more detailed experiments regarding the influence of the LED position for dry and wet membranes. The differentiation between these two membrane states is important because the liquid film on a wet membrane leads to higher reflection and thus a lower test line to background ratio.
It was found that the lightcone position is slightly favorable over the PCB position when it comes to evaluation of the ratio of MGVs of test lines and background, with an increase

of the MGV ratio of 2%. The experiment was done for fluorophore concentrations of 25 ng/cm and 100 ng/cm. Decrease in MGV ratio when changing from dry to wet membrane state did not depend on the LED position as the relative decrease was 13% and 28% for 25 ng/cm and 100 ng/cm, respectively, for PCB position and lightcone position alike. The MGVs for different parameters and membrane states for 25 ng/cm and 100 ng/cm can be seen in figure 29.

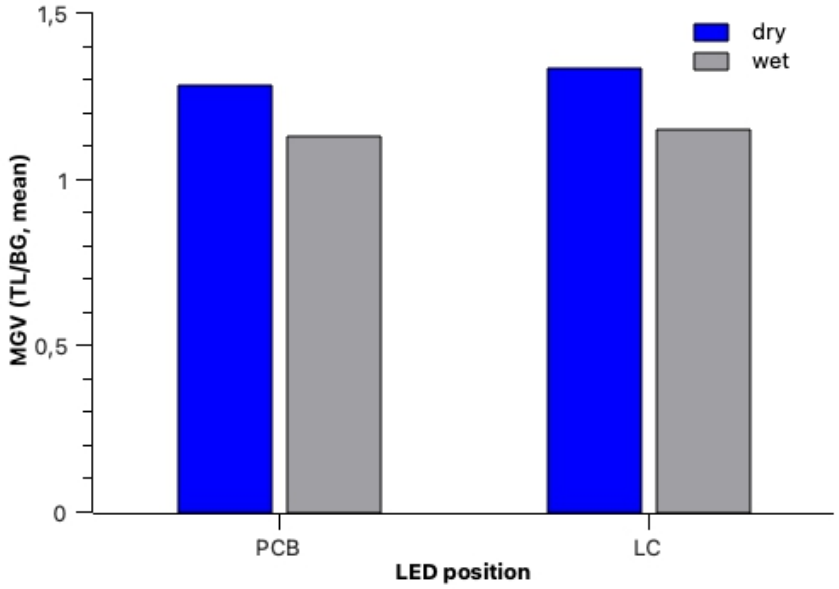

(a) 25 ng/cm

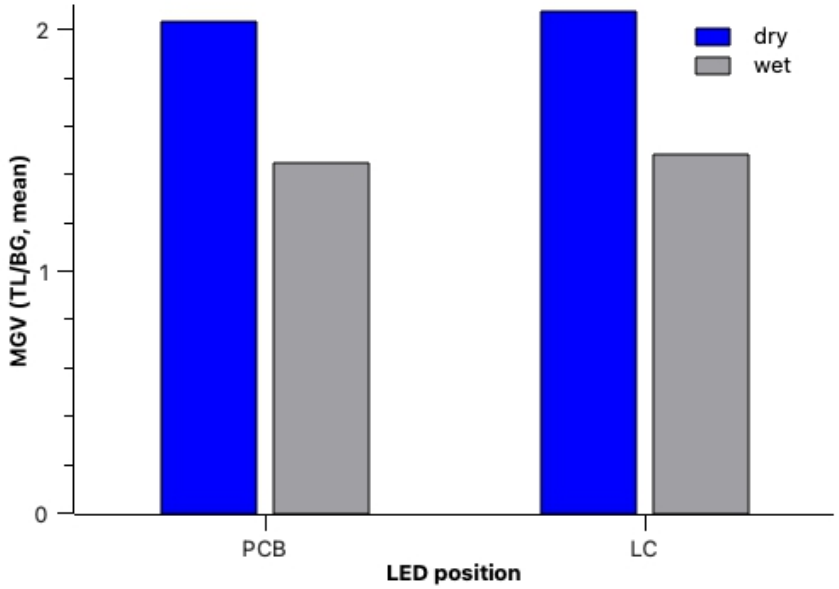

(b) 100 ng/cm

Figure 29: Comparison of Broadcom LED in PCB and lightcone position, in dry and wet membrane state; $t_{int} = 10$ ms, cassette used = ABSW

Even though lightcone position gives slightly higher MGVs, there are more factors to be considered when deciding on a final version of the Bloom FLURE Lab, like cost and additional steps that have to be taken in order to implement LEDs in lightcone position. A final decision on prototype design is made in chapter 3.2.5.

3.2.3. LED Position – Green LEDs

Implementing PCB positioning of UV-LEDs in future prototypes requires the reduction of the current amount of green LEDs found on the PCB. As AuNP read-out uses six green LEDs and future prototypes should be able to evaluate both, fluorescent and AuNP-based strips, it has to be determined that reducing the total number of green LEDs does not interfere with this process. Therefore, experiments testing the feasibility of implementing this solution were performed. It is to be decided only after analysis of the results if the option of placing the UV-LEDs on the main PCB should even be further investigated in this work.

To investigate the applicability of this setting, an experiment with a modified Bloom Lab with only four green LEDs was done. It was shown that calibration is still possible although it was found that integration time needs to be increased by more than 40% to achieve the same illumination as with six LEDs. This increase in integration time poses no problem in the regular use of the Bloom Lab but shall be noted for completeness. Illumination patterns achieved with four and six green LEDs can be seen in figure 30.

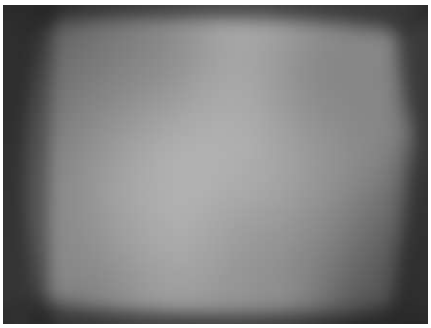

(a) four green LEDs

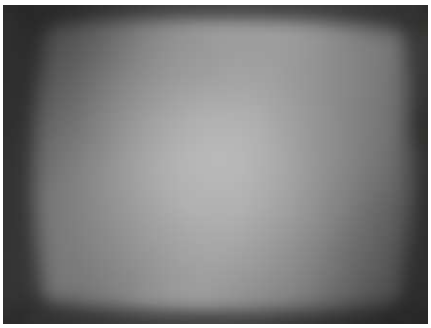

(b) six green LEDs

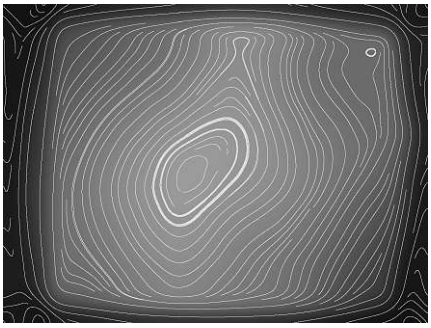

(c) four green LEDs – Intensity contours

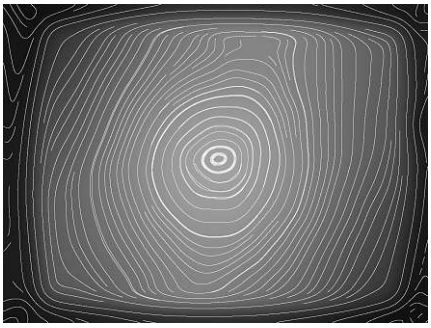

(d) six green LEDs – Intensity contours

Figure 30: Illumination of the calibration test strip with four green LEDs and six green LEDs

Figures 30(c) and (d) show the contours of the intensity profile obtained with four and six LEDs, respectively. It can be seen that six LEDs lead to more uniform illumination, as contour lines are more symmetrical than the contour lines achieved with four LEDs. In order to gain more information about the effects these differences have on the measurement process, a follow-up experiment was performed.

Two reference test strips (Senova) with a clearly defined test line (G4, G7 – see fig. 31) were measured with each version of the Bloom Lab. Both strips come with two lines with predefined intensities. The darker line on the right side of the strips is the reference control line, the other, lighter line corresponds to the reference test line. Both reference strips were inserted into both versions of the Bloom Lab and a measurement was started, similar to what happens during a testing flow with the Bloom System. The intensity of the reference lines was automatically measured. Measurements were repeated five times for every set of parameters (four green LEDs: G4, G7; six green LEDs: G4, G7).

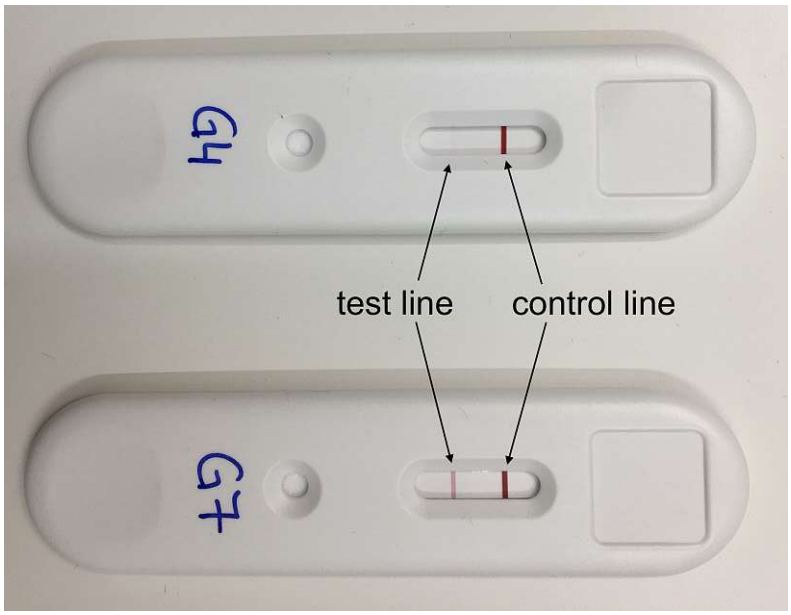

Figure 31: AuNP reference strips are usually used for investigations into measurement repeatability and stability. Each strip shows two lines, a dark reference control line (right) and a reference test line (left).

The automatic calculation of the reflected light done by the Bloom Lab showed a difference <1% between the same strip when measured with the Bloom Lab with four and six green LEDs, for both G4 and G7 reference strip. The repeatability of measurements performed with regular devices with six green LEDs is in the same range and typically <1%. The modified unit using only four green LEDs is thus within the acceptable limits to continue research as this proofs that regular Bloom Tests can be used and evaluated with both versions, not being influenced by the difference in illumination pattern. This is important for the decision on final parameters of the Bloom FLURE Lab.

3.2.4. Comparison of Prototypes

To further investigate different combinations of parameters, Prototype 1 and Prototype 3 were compared. This included an intrinsic comparison between OSRAM (Prototype 1) and Broadcom (Prototype 3) LED models as well as an investigation into whether lightcone position (Prototype 1) or PCB position (Prototype 3) is favorable. It was found that Prototype 3 (Broadcom LEDs, PCB position) shows higher illumination than Prototype 1 (OSRAM LEDs, lightcone position) as the MGV of the background as well as the control line-background ratio increased by 59%, when using the same integration time. With adjusting of the integration time such that the background shows the same MGV for both prototypes no significant increase of the control line/background ratio could be found. This leads to the conclusion that Broadcom and OSRAM LEDs are equally suitable for fluorophore excitation and differences in performance are not due to the peak wavelength but due to other LED parameters, e.g. the viewing angle. This underlines the results already presented (e.g. fig. 26).

As stronger illumination allows for shorter integration times which again lead to less noise, Prototype 3 is to be favored over Prototype 1. The results of section 3.2.2 that smaller LED viewing angles result in higher MGVs were repeated during prototype comparison. Prototypes 1 and 2 were compared by Junger in [16] where it was found that Prototype 2 gives lower MGVs than Prototype 1. When further exploring this comparison it can be said that Prototype 2 gives lowest MGVs, with the Luminus LED model having the widest viewing angle. Prototype 3, with the Broadcom LED model displaying the smallest viewing angle, results in highest MGVs.

3.2.5. Summary

A final decision was made to use Broadcom LEDs in PCB position for further experiments as this solution provides promising results also for a future FLURE Lab. Advantages include:

- Broadcom LEDs give highest MGVs
- Lower production costs due to reduction of amount of green LEDs

Although UV-LEDs in lightcone position give a slightly higher MGV during analysis, the difference is not substantial enough to compensate for the higher production costs. New lower lightcones would have to be designed and manufactured to be able to accommodate two UV-LEDs. When using only four green LEDs instead of six green LEDs costs can be further reduced.
Prototype 3 was thus found to possess the best combination of parameters.

3.3. LFIA Membrane

To further optimize fluorescent read-out, it is necessary to find the optimal membrane to be used for the immunoassay. The seven different membranes described in section 2.4 differ only in their effective pore size and their backing cards. In a first experiment each

membrane was inserted into a white ABS test cassette and reflectance and autofluorescence in dry state were measured with Prototype 3 (fig. 32).

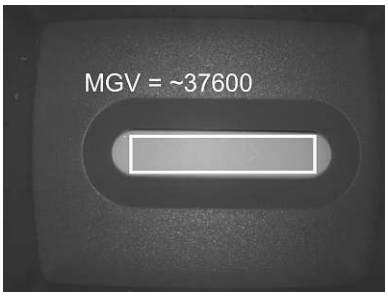

(a) CN95

(b) CN140

(c) CN150T

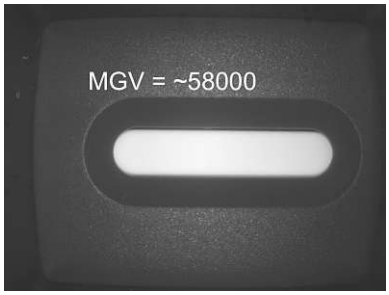

(d) CN150W

(e) HF120

(f) FF80

(g) FF120

Figure 32: Images of different bare membranes taken with Prototype 3 without optical longpass filter; $t_{int} = 5$ ms for all images, cassette used = ABSW; MGVs were calculated over a rectangular region of interest within the read-out window, as indicated in subfig. (a).

One membrane (CN150W) was labeled by the manufacturer as the best choice for fluorescent assays. The white backing allows for unfocused fluorescent light to be reflected from the backside of the assay which results in higher yield reaching the sensor. All membranes, except for CN150W, showed similar reflectance or autofluorescence with absolute MGVs between 34300 and 38600 (see fig. 32). As this measurement was interested in the "noise" being generated by each membrane, the comparison uses absolute mean-gray values without the division or substraction of any background.

The fact that CN150T exhibits different reflection properties than CN150W leads to the conclusion that the reflectance strongly depends on the backing card on which the different strip pads are assembled. Absolute MGV for CN150W was up to 70% higher than for all other membranes (MGV = 58000).

When using a longpass filter (GG475, Schott) signals from reflectance and autofluorescence could be decreased by more than 80%. As an example, two images of CN95 taken with an integration time of 10 ms, one without an optical filter and one using GG475, are compared in figure 33.

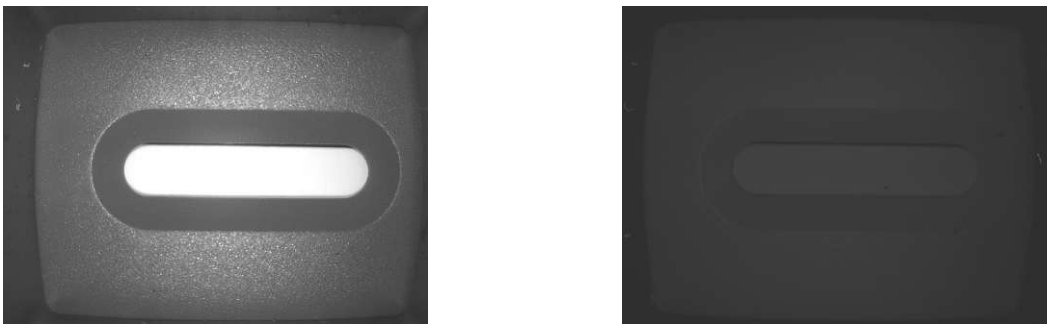

(a) without optical filter **(b)** with GG475

Figure 33: CN95 measured with Prototype 3, using (a) no filter and (b) GG475; t_{int} = 10 ms, cassette used = ABSW

As membranes are supposed to be used with liquid samples, reflectance and autofluorescence of wet membranes was also investigated. Again it was found that all membranes, except for CN150W, showed similar MGVs. Even when only wetting CN150W with MilliQ water without any fluorescent particles it is clearly visible that this combination of membrane and backing leads to strong reflection of light towards the sensor (fig. 34).

However, when leaving the wet membrane to dry no change in membrane structure or any residue can be observed once the membrane has fully dried. Therefore, we have to conclude that this strong signal is indeed due to the white backing card of CN150W.

As a result of this section's experiments it is clear that CN150W cannot be used with the current version of the Bloom FLURE Lab due to the high reflectance of the white backing card. As this combination was marked as most suitable for fluorescent assays by the manufacturer it is possible that the FLURE Lab would have to be adapted in order to be able to use time-resolved fluorescence. With this modification any unwanted noise by reflection could be eliminated from the signal.

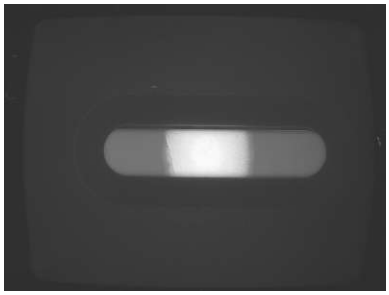

(a) CN150W with 2.5 µl MilliQ water

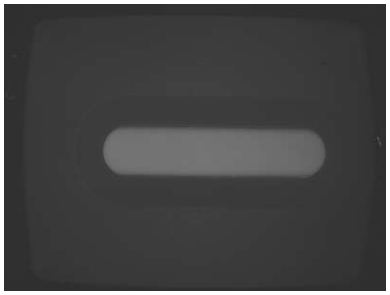

(b) CN150W, same strip post drying

(c) CN150T with 2.5 µl MilliQ water

Figure 34: (a) CN150W and (c) CN150T in wet state; (b) shows the same strip as in (a) after drying. t_{int} = 10 ms, cassette used = ABSW

With the current FLURE Lab all other combinations of membrane and backing cards were deemed functional. The difference in pore size between the various membranes does not affect the reflectance or autofluorescence. It can thus be said that the membrane for future fluorescent lateral flow assays can be chosen purely in accordance to the sample and desired flow speed.

3.4. Cassette Material

Similar to the membrane used, another factor affecting the SNR of fluorescent immunoassays is the autofluorescence and reflectance of the test cassette in which the assay itself is encased. The influence of test cassette material and color was investigated based on three different test cassettes (see section 2.5). A fluorescent reference strip was slid into the ABSW, ABSB and MAKR cassettes which were then inserted into the Bloom FLURE Lab. Three consecutive measurements were done with each cassette, after which the next cassette was inserted for measuring. This process was repeated three times in total to account for potential influence of the order of measurement. Resulting MGVs of the control line and the background were then averaged and divided. Figure 35 shows the results of this experiment.

Values in fig. 35 are not degradation-corrected as this correction is usually done with a linear fit (see section 2.7). However, the degradation of the reference strip in this experiment is best fitted with an exponential fit and it can be seen even from uncorrected data that ABSB gives higher contrast in every set of measurements. ABSB leads to up

to 37% increase of control line to background ratio correction compared to MAKR, after the application of a customized exponential degradation correction function. The relative increase in contrast between ABSB and ABSW is around 25%. The values measured using ABSB are continuously higher than the other sets of measurements. This shows that the increase in MGV is indeed due to the effects of the test cassette and independent of sample fluctuations or order of measurement.

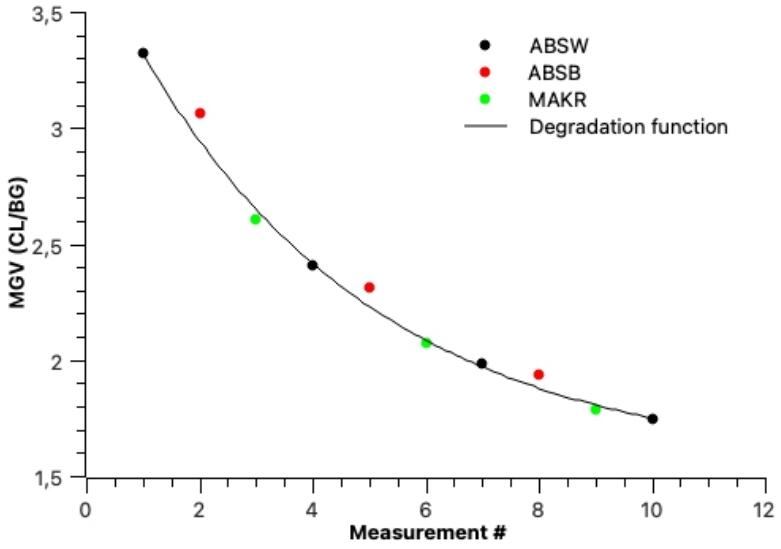

Figure 35: Cassette comparison using a fluorescent reference strip; degradation function: $y = 1.53 + 2.26 \cdot \exp(-x/4.26)$, $t_{int} = 15$ ms

It is clear that ABSB brings an improvement regarding the contrast of the read-out process of a fluorescent test strip in the Bloom FLURE Lab. This is most likely due to the decreased reflection and stray light caused by the black test cassette surface in comparison to the white surface of the regular Bloom test cassette.

In a next step, actual black ABS test cassettes could be produced to evaluate if the difference between black and white ABS still persists or if the increase in contrast might also be due to the additional layer of lacquer that was used to spray paint the existing white ABS test cassette black. Using these spray painted cassettes in a regular Bloom Test kit is definitely not a valid option as the lacquer splintered regularly during experiments and black dust had to be removed frequently from the membrane in order not to falsify evaluation of mean gray values of test and control lines. ABS as the test cassette material might also be changed in future versions of Bloom FLURE Tests as additional functions could be added, e.g. external temperature control via the test cassette. Functionality of ABS for these future improvements and alterations would have to be investigated separately. In the current version of the Bloom FLURE Lab black ABS test cassettes seem to be the best option, based on the data that was collected and evaluated so far. Any choices of test cassette material not depending on the pure physical factors like design compatibility, ease of production, etc. shall not be evaluated in this thesis as they are purely depending on marketing and financial decisions.

3.5. Fluorophore Testing

This chapter summarizes the results of experiments conducted with other fluorescent materials than the regularly used fluorescence reference strips. Y_2O_3:Eu powder was chosen as a material of interest due to its increased stability under UV irradiation (see section 1.3.5) which makes it a highly promising candidate for the use with fluorescent LFIAs. This section also shows the findings of the experiments on the feasibility of the read-out of commercially available fluorescent LFIAs with the FLURE Lab Prototypes.

3.5.1. Y_2O_3:Eu – Dissolution

In a first experiment, dissolution of Y_2O_3:Eu was tried in 1×PBS buffer of different pH values at different concentrations (0.5 g/ml, 0.05 g/ml, 0.005 g/ml). PBS was chosen as a suitable buffer as it is often used with lateral flow membranes and is known for its compatibility with immunoassays. The two 1×PBS solutions had pH 7.4 which corresponds to the natural pH value of blood samples and pH 9.5 which is closer to the optimal pH for stability of yttrium-oxide solutions (pH10) [35]. After addition of buffer to the powder, solutions stayed opaque even after continuous vortexing and a 60°C water bath and powder residue formed quickly.

Upon further literature research dissolution was tried in 6M HCl [36]. Solutions of 0.01 g/ml, 0.1 g/ml, 0.2 g/ml and 0.3 g/ml were prepared, vortexed and put in a 60°C water bath for 30 minutes to accelerate the process. However, all prepared solutions stayed opaque, meaning the oxide was only resuspended and had not yet dissolved.
After a period of one week, during which samples were vortexed once a day, the 0.1 g/ml solution appeared transparent again, indicating full dissolution of the sample. Two more weeks later the 0.2 g/ml solution was fully transparent as well. The 0.3 g/ml solution did not clear up completely. Residue was found at the bottom of the Eppendorf tube even several weeks after preparation. The entirely dissolved samples of 0.1 g/ml and 0.2 g/ml were then tested for their fluorescent properties, using Prototype 3 and a spectrofluorometer (Tecan Spark10M Multi Mode Microplate Reader).

(a) 0.2 g/ml, CN150T **(b)** 0.2 g/ml, CN150W

Figure 36: 0.2 g/ml Y_2O_3:Eu in HCl on CN150 LFIA membrane with (a) transparent and (b) white backing, dry state; tested in Prototype 3, t_{int} = 10 ms, cassette used = ABSW

As can be seen in fig. 36(a) no fluorescent signal is visible for CN150T. The white backing of CN150W leads to much higher overall reflection in fig. 36(b), similar to results found in section 3.3. All other experiments where yttrium-oxide solutions were tested in Prototype 3 showed the same results, with no fluorescent signal, independent of the concentration used, membrane (except for CN150W) or drying method (incubator or room temperature). It remains questionable if the signal obtained from measurements of CN150W is indeed a fluorescent signal or just noise due to increased reflectivity. When looking at the membrane, it was visible that the fluorophore solution had only formed a coating on the membrane surface and that the fluorophores had not been absorbed. Due to the fact that the signal depends so strongly on the backing card, it is possible that the backing itself is the reason for the signal. This would also mean that the prepared fluorophore solutions are not functional at all or not excitable with the light source used in the experiment.

The key findings of this section are:

- Dissolution of Y_2O_3:Eu in 6M HCl under the described parameters is a very slow and only partially successful process.
- The resulting solutions do not exhibit fluorescent properties under UV illumination in Prototype 3.
- The obtained signal is strongly dependent on the backing card of the membrane used and is most likely only the reflection of LED light.

3.5.2. Y_2O_3:Eu – Excitation Wavelength

One hypothesis to explain the inability of Prototype 3 to excite fluorescence of Y_2O_3:Eu is the wavelength of the UV-LEDs. A spectrofluorometer (Tecan Spark10M Multi Mode Microplate Reader) was thus used to find the optimal wavelength for fluorophore excitation in solution. The three tested wavelengths were 254 nm (excitation wavelength of Y_2O_3:Eu), 333 nm (excitation wavelength of europium) and 365 nm (peak wavelength of OSRAM, Luminus and Broadcom LEDs). Solutions were not only tested for their fluorescent response but also for their degradation as each well was exposed to the light source three times in a row.

Figure 37 shows the emission curves for all solutions at the chosen wavelengths. Full lines correspond to the first measurement, broken lines to second and dotted lines to the third. Solutions seem to be rather stable, the exceptions being 0.1 g/ml at 254 nm and 0.2 g/ml at 365 nm. Pure 6M HCl was also tested to guarantee that there is no unknown background component coming from the acid.

Figures 37b and 37c show a clear increase of signal with higher fluorophore concentration. Figure 37a shows no significant difference between the two concentrations in the region of interest but a pronounced local peak at around 590 nm for 0.2 g/ml whereas 0.1 g/ml does not show such a peak.

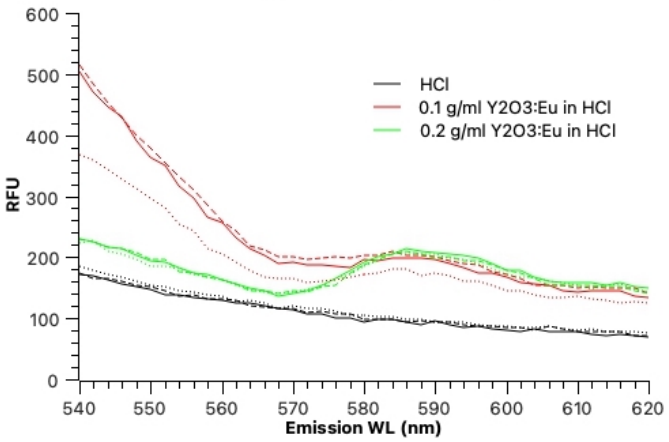

(a) 254 nm

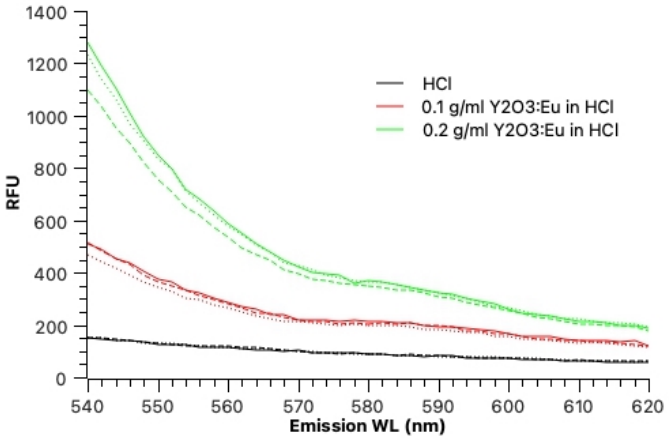

(b) 333 nm

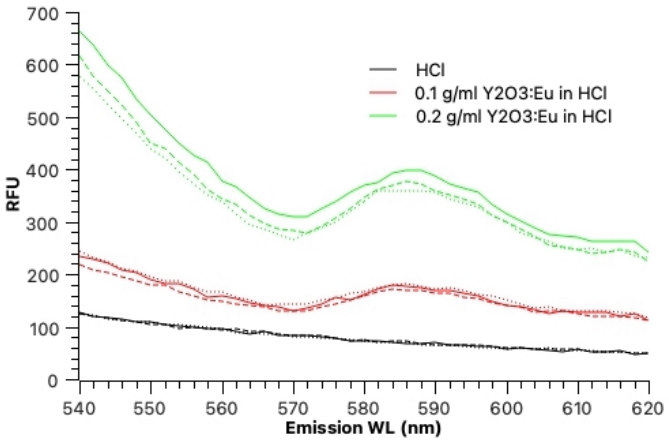

(c) 365 nm

Figure 37: Testing of fluorophore solutions under different wavelengths; RFU – relative reflective unit

At 333 nm (fig. 37b) the graph is a decreasing function and shows no peak. Even though the graphs in figures 37a and 37c show local maxima that can be interpreted as fluorescent peaks it is questionable if this material is to be used in further experiments as this peak might get lost in the high noise when measuring overall light-intensity and not scanning over different emission wavelengths.
Furthermore, it is unclear if the shift of the emission wavelength (612 nm) to lower wavelengths is due to the dissolution of the sample or due to an entirely different reason. The overall signal intensity at a local peak is highest for excitation with 365 nm, at around 400 RFU.

The results of this subsection can be summarized as follows:

- 365 nm is a suitable wavelength for excitation of fluorescence of europium-doped yttrium oxide.
- As the in-built UV-LEDs in Prototype 3 (Broadcom) have their peak wavelength at 365 nm, the lack of fluorescence signal in experiments with Prototype 3 is most likely due to the UV light flux provided by the LEDs but not due to their wavelength.
- With a different light source of the same wavelength in the spectrofluorometer detection of a fluorescent signal is possible, most likely due to stronger illumination.
- Signal shape and intensity obtained from spectrofluorometer measurements are not clear and high enough to decide on the permanent usage of Y_2O_3:Eu.

3.5.3. Y_2O_3:Eu – Compatibility with Different LED Models

Another set of experiments was conducted to assess the capability of each LED model to excite the undissolved fluorescent powder. Results should give a hint if fluorescence activity is low due to the oxide's dissolution state. For this bare, undissolved Y_2O_3:Eu powder was illuminated with an individual, hand-held UV-LED.

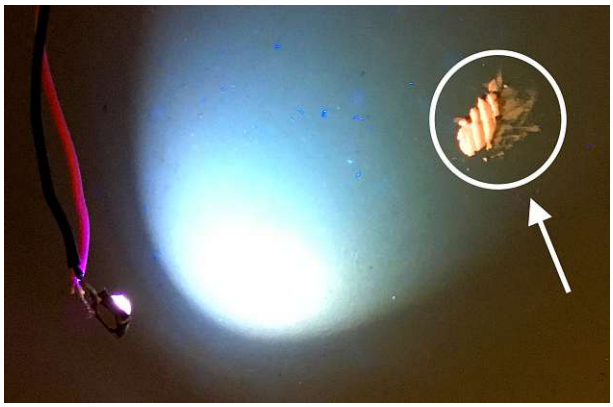

Figure 38: Y_2O_3:Eu powder (white circle and arrow) being illuminated by a hand-held UV-LED, showing expected red fluorescent light. On the left side the UV-LED with cables is visible. The bright spot in the middle is the reflection of UV light by the surface on which the experiment was performed.

Upon illumination of the sample the oxide powder lit up bright red (see fig. 38), the expected color for fluorescence of this material [37].

The only LED for which the powder did not fluoresce was the LED model by IBT, with a peak wavelength of 340 nm. The intensity of fluorescence depended on the LED and was only assessed visually but not quantified as this test should only provide a yes or no answer regarding the possibility of exciting the fluorophore with each LED model. This again gives a hint that the the problems of fluorophore excitation in Prototype 3 are not due to LED wavelength or the oxide itself. Problems might thus be caused by LED placement or fluorophore dissolution state.

To test this hypothesis Y_2O_3:Eu powder was glued to an LFIA membrane (CN150W) which was then tested in Prototype 3 (see fig. 39). The strip showed high reflectance where bare glue was exposed to the light source. The areas with glued-on powder appeared almost dark, exhibiting lower reflectance but also no fluorescence. Again, results give rise to the conclusion that the UV flux provided by Broadcom LEDs in PCB position is not sufficient to excite this fluorophore.

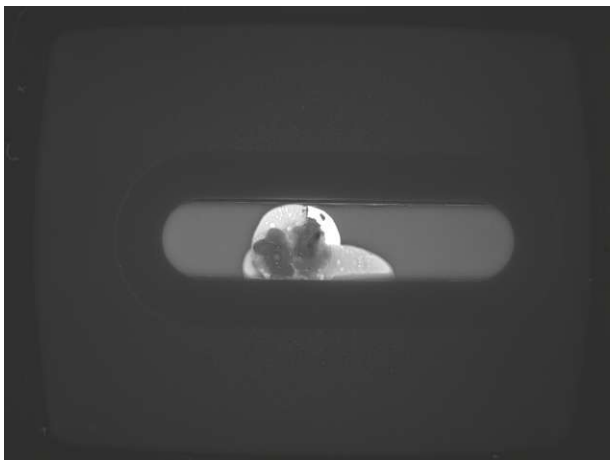

Figure 39: CN150W membrane with glued on powder in Prototype 3; Bright areas correspond to bare glue, dark areas to glued-on powder. t_{int} = 10 ms, cassette used = ABSW

It is possible that excitation is visible once the fluorophore has been properly dispensed onto the membrane. Machinery for this production was not available for this thesis. Due to the findings presented in this section, further experiments with Y_2O_3:Eu solutions were discontinued.

3.5.4. AllTest TSH Test Strip

In order to get information on the compatibility of regular, available fluorescent LFIAs and the Bloom FLURE Lab Prototype 3, TSH test strips by AllTest were used (fig. 40). These LFIA strips are declared by the manufacturer to be used to measure TSH in serum or plasma in a range of 0.1 - 100 µIU/ml. For more information see Appendix fig. 50.

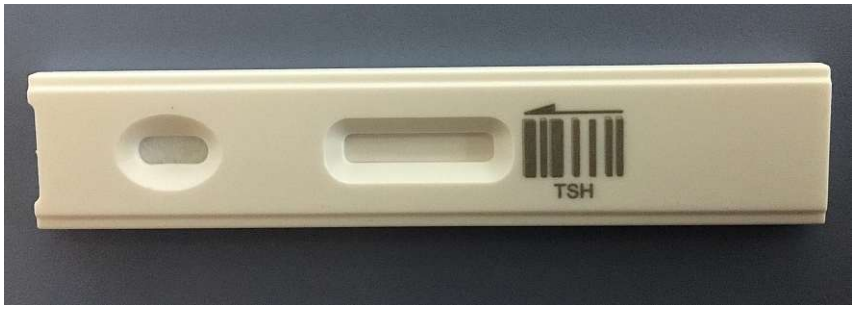

Figure 40: AllTest TSH test strip; samples are applied in the sample application window on the left side, the read-out window is located in the middle of the test strip cassette.

In a first test and due to the unavailability of any spiked biological sample, tests were performed with spiked buffer only. TSH antigen was diluted to six different concentrations in Bloom's TSH Test running buffer. To get a good overview of the measurement range, samples showed a concentration of 0.1, 1, 4, 16, 32 and 65 µIU/ml. 75 µl of each sample were then mixed with 75 µl of AllTest reaction buffer and 75 µl of this mixture were applied onto the sample pad of the test. Directly after sample application, tests were put in a light-shielded drawer and incubated for 15 minutes. After incubation, test strips were taken out of the cassette. They were then cut to the correct size, inserted into a white ABS test cassette and measured with Prototype 3. After checking the background with a bare strip, 10 ms were set as a proper integration time.

The results are presented in fig. 41.

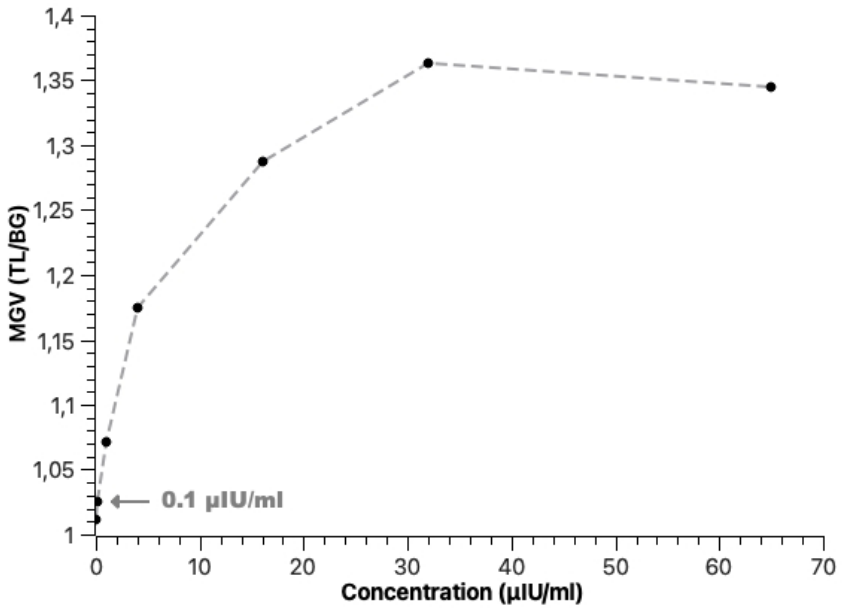

Figure 41: Testing of TSH antigen in buffer with AllTest TSH strips and Prototype 3. t_{int} = 10 ms, cassette used = ABSW

Fig. 41 shows a clear difference in fluorescent signal for sample concentrations between 0.1 and 32 µIU/ml. The fact that signal intensity is a function of the analyte concentration is expected and shows that the read-out of the strips used is indeed possible with Prototype 3. The next higher sample (64 µIU/ml) shows no increase and therefore hints at a state of saturation reached by the LFIA membrane. This is most likely due to the different matrix used in the experiment as this test strip is usually to be used with plasma or serum. As TSH levels are considered elevated above a value of 4 µIU/ml, the measurement range is nevertheless deemed sufficient for a first test. The first data point in fig. 41 shows the baseline value of a wet strip where only 75 µl of buffer were applied. Error bars of 15%, which is the error of the test strip as stated by the supplier, were not included in this graph.

In a next step the experiment should be repeated with serum or plasma as stated in the instructions for use of the test strip. Using spiked reference samples should give a better idea if read-out of this LFIA strip is doable with Prototype 3. Additionally, all future tests should include multiple read-outs of the same strip as only with this data it becomes possible to investigate the repeatability of the read-out process. In the first experiment combining fluorescent lateral flow strips available on the market and the FLURE Lab the focus lay on the actual functionality of this combination. Only after assessing that it is indeed possible to use strips from another supplier with the FLURE Lab further experiments should be done.

4. Summary and Outlook

This thesis has shown several areas for improvement of the Bloom FLURE Lab and its components:

- Use of Broadcom UV-LED model AUV3-SQ32-0RT0K enables image capture with optimal contrast, while ideal integration time depends on the test line intensity
- Integration of the UV-LEDs on the main PCB does not significantly reduce image contrast and leads to lower production cost and effort
- Use of an optical longpass filter GG475 is necessary to avoid early saturation
- Autofluorescence and reflectance do not depend on the LFIA membrane structure or pore size but vary greatly with the chosen backing card
- Black ABS test cassettes allow for higher contrast compared to regular white ABS test cassettes

It was also found that the Bloom FLURE Lab is able to read out fluorescent LFIAs by other suppliers. This is necessary and useful in order to establish a wide test portfolio without having to create every new test strip from scratch.

Future research should be conducted on the following topics:

- Addition of an emission filter for the UV-LEDs to maximize signal-to-noise ratio
- Replacement of GG475 by a custom-made band-pass filter to minimize stray UV light reaching the sensor (Experiments with such a filter where initially planned to be conducted within the scope of this thesis but could not be finished due to problems with the supplier.)
- Implementation of time-resolved fluorescence to increase image contrast by shutting out all autofluorescence and reflective components of the signal
- Use of an image stacking algorithm in combination with images taken at different integration times to maximize the read-out range for weak and strong signals

Future development targets could also include the implementation of an external temperature-control mechanism for the test strip to improve test precision.

Some of these further improvements come with limitations and difficulties that need to be considered in future research.
When adding an emission filter to the UV-LEDs the positioning on the main PCB could raise a problem regarding available space as the additional filter must not negatively influence performance of the green LEDs. If it is found in future experiments that the addition of an emission filter brings much higher contrast and it is not possible to implement it due to LED position, LEDs could be moved to the lower lightcone. This positioning would offer more space but also comes with higher production costs and significant design changes.
Adding temperature control to the Bloom FLURE Lab and setting it to 37°C to 40°C would lead to increased stability of the immunoreaction on the test membrane. This would

increase repeatability and test precision but as fluorescent signal intensity decreases with increasing temperature additional experiments would be necessary [38, 39, 40, 41]. These experiments should strongly focus on the evaluation of benefits in regards to the overall sensitivity of the test when using higher temperatures.

References

[1] E. Kaniusas, *Biomedical signals and sensors*. Biological and medical physics, biomedical engineering, Heidelberg: Springer, 2012.

[2] D. Haarburger and T. S. Pillay, "Historical perspectives in diagnostic clinical pathology: development of the pregnancy test," *Journal of Clinical Pathology*, vol. 64, pp. 546–548, June 2011.

[3] E. Juntunen, T. Myyryläinen, T. Salminen, T. Soukka, and K. Pettersson, "Performance of fluorescent europium(III) nanoparticles and colloidal gold reporters in lateral flow bioaffinity assay," *Analytical Biochemistry*, vol. 428, pp. 31–38, Sept. 2012.

[4] J. D. Bishop, H. V. Hsieh, D. J. Gasperino, and B. H. Weigl, "Sensitivity enhancement in lateral flow assays: a systems perspective," *Lab on a Chip*, vol. 19, no. 15, pp. 2486–2499, 2019.

[5] B. O'Farrell, "Lateral Flow Technology for Field-Based Applications—Basics and Advanced Developments," *Topics in Companion Animal Medicine*, vol. 30, pp. 139–147, Dec. 2015.

[6] F. Di Nardo, M. Chiarello, S. Cavalera, C. Baggiani, and L. Anfossi, "Ten Years of Lateral Flow Immunoassay Technique Applications: Trends, Challenges and Future Perspectives," *Sensors*, vol. 21, p. 5185, July 2021.

[7] K. J. Land, D. I. Boeras, X.-S. Chen, A. R. Ramsay, and R. W. Peeling, "REASSURED diagnostics to inform disease control strategies, strengthen health systems and improve patient outcomes," *Nature Microbiology*, vol. 4, pp. 46–54, Jan. 2019.

[8] J. H. Soh, H.-M. Chan, and J. Y. Ying, "Strategies for developing sensitive and specific nanoparticle-based lateral flow assays as point-of-care diagnostic device," *Nano Today*, vol. 30, p. 100831, Feb. 2020.

[9] Y. Huang, T. Xu, W. Wang, Y. Wen, K. Li, L. Qian, X. Zhang, and G. Liu, "Lateral flow biosensors based on the use of micro- and nanomaterials: a review on recent developments," *Microchimica Acta*, vol. 187, p. 70, Jan. 2020.

[10] J. H. W. Leuvering, P. J. H. M. Thal, M. v. d. Waart, and A. H. W. M. Schuurs, "Sol particle agglutination immunoassay for human chorionic gonadotrophin," *Fresenius' Zeitschrift für analytische Chemie*, vol. 301, pp. 132–132, Jan. 1980.

[11] V. Amendola, R. Pilot, M. Frasconi, O. M. Maragò, and M. A. Iatì, "Surface plasmon resonance in gold nanoparticles: a review," *Journal of Physics: Condensed Matter*, vol. 29, p. 203002, May 2017.

[12] C. Parolo, A. Sena-Torralba, J. F. Bergua, E. Calucho, C. Fuentes-Chust, L. Hu, L. Rivas, R. Álvarez Diduk, E. P. Nguyen, S. Cinti, D. Quesada-González, and A. Merkoçi, "Tutorial: design and fabrication of nanoparticle-based lateral-flow immunoassays," *Nature Protocols*, vol. 15, pp. 3788–3816, Dec. 2020.

[13] R. Raliya, D. Saha, T. S. Chadha, B. Raman, and P. Biswas, "Non-invasive aerosol delivery and transport of gold nanoparticles to the brain," *Scientific Reports*, vol. 7, p. 44718, Mar. 2017.

[14] "Sigma Aldrich: Gold nanoparticles."

[15] S. A. Maier, *Plasmonics: fundamentals and applications*. New York: Springer, 2007.

[16] P. Junger, "Development and Integration of a Quantitative Readout for Fluorescence-based LFIAs," Master's thesis, Universität Stuttgart, Mar. 2022.

[17] B. N. Khlebtsov, R. S. Tumskiy, A. M. Burov, T. E. Pylaev, and N. G. Khlebtsov, "Quantifying the Numbers of Gold Nanoparticles in the Test Zone of Lateral Flow Immunoassay Strips," *ACS Applied Nano Materials*, vol. 2, pp. 5020–5028, Aug. 2019.

[18] Z. Gryczynski and I. Gryczynski, *Practical fluorescence spectroscopy*. Boca Raton: CRC Press, 2020.

[19] J. R. Lakowicz, *Principles of fluorescence spectroscopy*. New York: Springer, 3rd ed ed., 2006.

[20] G. C. Cox, ed., *Fundamentals of fluorescence imaging*. Singapore: Jenny Stanford Publishing, 2018.

[21] Urusov, Zherdev, and Dzantiev, "Towards Lateral Flow Quantitative Assays: Detection Approaches," *Biosensors*, vol. 9, p. 89, July 2019.

[22] F. Wang, W. B. Tan, Y. Zhang, X. Fan, and M. Wang, "Luminescent nanomaterials for biological labelling," *Nanotechnology*, vol. 17, pp. R1–R13, Jan. 2006.

[23] M. H. Werts, "Making sense of Lanthanide Luminescence," *Science Progress*, vol. 88, pp. 101–131, May 2005.

[24] L. Crawford, J. Higgins, and D. Putnam, "A Simple and Sensitive Method to Quantify Biodegradable Nanoparticle Biodistribution using Europium Chelates," *Scientific Reports*, vol. 5, p. 13177, Sept. 2015.

[25] F. Scientific, "Product Specification: Fluoro-Max Fluorescent Beads with Europium Chelate," 2017.

[26] J. He, C. Li, L. Ding, Y. Huang, X. Yin, J. Zhang, J. Zhang, C. Yao, M. Liang, R. P. Pirraco, J. Chen, Q. Lu, R. Baldridge, Y. Zhang, M. Wu, R. L. Reis, and Y. Wang, "Tumor Targeting Strategies of Smart Fluorescent Nanoparticles and Their Applications in Cancer Diagnosis and Treatment," *Advanced Materials*, vol. 31, p. 1902409, Oct. 2019.

[27] J. Zhou, P. Jangili, S. Son, M. S. Ji, M. Won, and J. S. Kim, "Fluorescent Diagnostic Probes in Neurodegenerative Diseases," *Advanced Materials*, vol. 32, p. 2001945, Dec. 2020.

[28] "BMG Labtech: Time-resolved fluorescence."

[29] A. P. Demchenko, "Photobleaching of organic fluorophores: quantitative characterization, mechanisms, protection," *Methods and Applications in Fluorescence*, vol. 8, p. 022001, Feb. 2020.

[30] J. Walish, J. Cox, J. Boone, J. Stone, N. Henderson, M. Maloney, J. Ma, J. Maa, N. On, K. Petre, B. G. Goodwin, S. Sozhamannan, and R. Deans, "Halo—A Universal Fluorescence Reader Based Threat Agent Detection Platform—A Proof of Concept Study Using SARS-CoV-2 Assays," *Frontiers in Public Health*, vol. 10, p. 852083, Apr. 2022.

[31] G. Rajakumar, L. Mao, T. Bao, W. Wen, S. Wang, T. Gomathi, N. Gnanasundaram, M. Rebezov, M. A. Shariati, I.-M. Chung, M. Thiruvengadam, and X. Zhang, "Yttrium Oxide Nanoparticle Synthesis: An Overview of Methods of Preparation and Biomedical Applications," *Applied Sciences*, vol. 11, p. 2172, Mar. 2021.

[32] C. Jurischka, F. Dinter, A. Efimova, R. Weiss, J. Schiebel, C. Schulz, B. Fayziev, P. Schierack, T. Fischer, and S. Rödiger, "An explorative study of polymers for 3D printing of bioanalytical test systems," *Clinical Hemorheology and Microcirculation*, vol. 75, pp. 57–84, July 2020.

[33] "Elliott Scientific: Schott GG475 12.5 mm diameter," Dec. 2022.

[34] Merck, "Product Specification: Yttrium oxide, europium doped."

[35] S. Santos, L. Setz, C. Yamagata, and S. R. H. de Mello-Castanho, "Rheological Study of Yttrium Oxide Aqueous Suspensions," *Materials Science Forum*, vol. 660-661, pp. 712–717, Oct. 2010.

[36] W. M. Haynes, *CRC Handbook of Chemistry and Physics, 95th Edition*. Hoboken: CRC Press, 95th ed ed., 2014.

[37] J. Jayaramaiah, B. Lakshminarasappa, and K. Nagabhushana, "Luminescence performance of europium-doped yttrium oxide thin films," *Journal of Luminescence*, vol. 157, pp. 63–68, Jan. 2015.

[38] J. Lou, T. M. Finegan, P. Mohsen, T. A. Hatton, and P. E. Laibinis, "Fluorescence-Based Thermometry:Principles and Applications," *Reviews in Analytical Chemistry*, vol. 18, Jan. 1999.

[39] H. Peng, M. I. J. Stich, J. Yu, L.-n. Sun, L. H. Fischer, and O. S. Wolfbeis, "Luminescent Europium(III) Nanoparticles for Sensing and Imaging of Temperature in the Physiological Range," *Advanced Materials*, vol. 22, pp. 716–719, Feb. 2010.

[40] D. Ross, M. Gaitan, and L. E. Locascio, "Temperature Measurement in Microfluidic Systems Using a Temperature-Dependent Fluorescent Dye," *Analytical Chemistry*, vol. 73, pp. 4117–4123, Sept. 2001.

[41] W. R. Ware and B. A. Baldwin, "Effect of Temperature on Fluorescence Quantum Yields in Solution," *The Journal of Chemical Physics*, vol. 43, pp. 1194–1197, Aug. 1965.

A. Datasheets

www.osram-os.com

LT T64G

TOPLED® Black

TOPLED Black is especially designed for variable message signs (VMS) and price changers. The black package offers premium contrast for display panels.

Applications

– VMS

Features:

– Package: black PLCC-2 package, colorless resin
– Chip technology: UX:3
– Typ. Radiation: 30°
– Color: λ_{dom} = 532.0 nm (• true green)
– Corrosion Robustness Class: 3B
– ESD: 2 kV acc. to ANSI/ESDA/JEDEC JS-001 (HBM, Class 2)

1 Version 1.3 | 2020-07-15

OSRAM
Opto Semiconductors

Figure 42: Datasheet of green OSRAM LEDs used for the analysis of AuNP-based LFIAs

www.osram.us/ledengin

Light is OSRAM

OSRAM

Our Brand
LED ENGIN

LuxiGen™ 365nm UV LED Gen 4 Emitter

LZ1-00UV0R

Key Features

- Highest flux density 365nm UV LED emitter
- Ultra-small foot print – 4.4mm x 4.4mm
- Surface mount ceramic package with integrated glass lens
- Very low Thermal Resistance (4.2°C/W)
- JEDEC Level 1 for Moisture Sensitivity Level
- Lead (Pb) free and RoHS compliant
- Emitter available on star MCPCB (optional)

Typical Applications

- Curing
- Currency verification
- Dental
- Fluorescence microscopy
- Forensics
- Inspection
- Leak detection
- Medical
- Sterilization

Figure 43: Datasheet of OSRAM LZ1-00UV0R UV-LED used in the Bloom FLURE Lab Prototype 1

LUMINUS

SST-10-UV Product Datasheet

SST-10-UV

Surface Mount UV LED

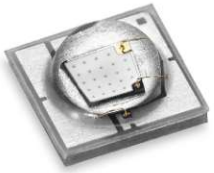

Table of Contents

Features:

- High Power UV LED with peak wavelengths 365 nm, 385 nm, 395 nm and 405 nm
- Industry standard 3.5 mm x 3.5 mm package
- 130° viewing angle
- Low Thermal Resistance : 1.4 °C/W
- Built-in ESD Protection
- Environmentally friendly: REACH, RoHS and Halogen compliant

Applications:

- Curing- inks, coating and adhesives
- Photocatalytic air/water purification
- Medical and Analytic instrumentation
- Diagnostics
- Fluorescence Imaging

Luminus Devices, Inc. • T 408.708.7000 • www.luminus.com
1145 Sonora Court, Sunnyvale, CA 94086 USA

Figure 44: Datasheet of Luminus SST-10-UV UV-LED used in the Bloom FLURE Lab Prototype 2

BROADCOM®

Data Sheet

AUV3-Sxx2-0xx0K

3W 3535 Surface-Mount UV LED

Description

The Broadcom® 3W 3535 surface-mount UV LEDs are energy-efficient LEDs that can be driven with high currents and can dissipate heat efficiently, resulting in higher reliability. Their low-profile package design addresses a wide variety of applications where superior robustness and high efficiency are required. They are packaged with ceramic-based materials, and the quartz lens on top of the package provides the product longevity needed for the respective end applications.

To facilitate easy pick-and-place assembly, the LEDs are packed in tape and reel. Each reel is shipped in a single flux and single color bin to ensure close uniformity.

Features

- High-reliability package with quartz lens.
- High-radiant flux output using InGaN dice technology.
- Available in 360-nm to 400-nm wavelength range.
- Available in 35° and 60° viewing angles.
- Compatible with the reflow soldering process.
- JEDEC MSL 1

Applications

- Industrial curing
- Photocatalyst purification
- Medical applications
- Horticulture

CAUTION! This LED is ESD sensitive. Observe appropriate precautions during handling and processing. Refer to the *Premium InGaN LEDs: Safety Handling Fundamentals ESD Application Note*, AN-1142, for additional details.

Figure 45: Datasheet of Broadcom AUCV3-SQ32-0RT0K UV-LED used in the Bloom FLURE Lab Prototype 3

SEOUL SEOULVIOSYS

CA3535 - CUD1GF1A

Deep UV LED - 310nm

UV CA3535 series (CUD1GF1A)

CUD1GF1A

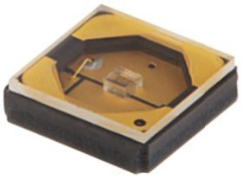

RoHS

Product Brief

Description

CUD1GF1A is a deep ultraviolet light emitting diode with peak emission wavelengths from 305nm to 315nm.

The LED is sealed in Ceramic packages including an optical transparent window.

It incorporates state of the art SMD design and low thermal resistance.

CUD1GF1A is designed for air and water sterilization and tools including chemical and biological analysis in that spectral range.

Features and Benefits

- Deep ultraviolet LED
- Low thermal resistance
- SMT solderable
- Lead Free product
- RoHS compliant

Key Applications

- Disinfection
- Fluorescent spectroscopy
- Chemical and Biological analysis

Figure 46: Datasheet of Neumüller CUD1GF1A UV-LED

IBT

IBT-L3535-UV-340nm
Product Datasheet

IBT-L3535-UV

UV LED 340nm

RoHS

Product Descriptions

- This product is UVC LED diode.
- Package size: 3.8X3.8mm.
- Quartz glass dome cover.
- Wavelength: 340nm.
- The package design coupled with careful selection of component materials allows the product to perform with good reliability.

Features:

- High Power UVA LED with Emission Wavelength Between 330nm and 345nm
- Compact Form Factor: 3.8 mm x 3.8mm Package
- Beam Angle of 30 / 60 degrees with dome cover
- High Reliability Package
- Standard SMD Process
- RoHS and REACH compliant

Applications

- Bio-Analysis
- Detection
- Sensor application
- Phototherapy
- Medical Spectroscopy

Ivy Bridge Technology Co., LTD. www.uvledchip.com Block 1, Third industrial park, Tangwei guangming District, Shenzhen, China 518132

Figure 47: Datasheet of IBT IBT-L3535-UV UV-LED

Data Sheet

SCHOTT

GG475

Optical properties	
Reflection factor	
P_d	= 0,918
Spectral values guaranteed (d = 3 mm)	
λ_c (τ_i = 0,5)	= 475 nm ± 6 nm
λ_s ($\tau_{i,U}$ = 1E-05)	= 410 nm
λ_p ($\tau_{i,L}$ = 0,92)	= 550 nm
Refractive indices	
n_d (587,6 nm)	= 1,52
n_s (852 nm)	= 1,52
n_t (1014 nm)	= 1,51
Sellmeier coefficients	
on request	
Internal quality	
Bubble class	3

Mechanical properties	
Reference thickness	
d	= 3,00 mm
Density	
ρ	= 2,56 g/cm³
Knoop hardness	
$HK_{[0.1/20]}$	= 451

Thermal properties		
Transformation temperature		
Tg	= 531 °C	
Thermal expansion in		10^{-6}/K
$\alpha_{(-30°C/+70°C)}$	= 8,2	
$\alpha_{(20°C/300°C)}$	= 9,4	
Temperature coefficient		
Tk	= 0,09	nm/K

Chemical properties	
Chemical resistance	
FR class	= 0
SR class	= 1
AR class	= 1
Resistance against humidity	
Resistant glass	
see pocket catalogue "Optical Filter Glass 2020", chapter 5.5	

Colormetric properties		1 mm	2 mm	3 mm
Illuminant D65	x	0,381	0,394	0,401
	y	0,463	0,485	0,494
	Y	89,5	88,5	87,7
	λ_d	568 nm	569 nm	569 nm
	P_e	0,567	0,664	0,709
Illuminant A	x	0,483	0,489	0,492
	y	0,453	0,460	0,463
	Y	90,7	90,0	89,4
	λ_d	580 nm	580 nm	580 nm
	P_e	0,560	0,648	0,689

Notes
Stricking glass
Longpass filter
DIN 58131
Disclaimer
All data without tolerances are to be understood to be reference values.

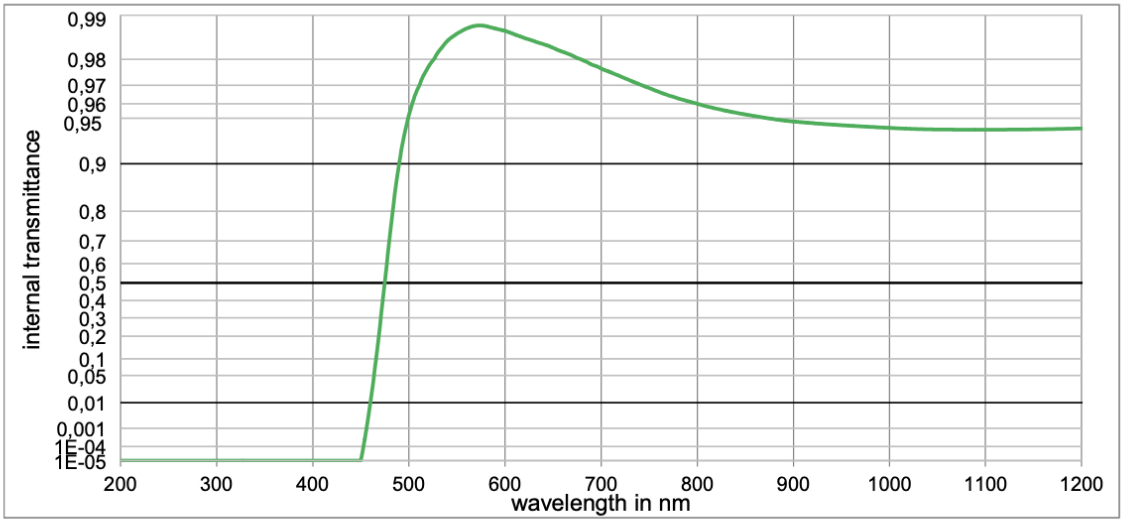

Status 18.11.2020 Page 1/2

Figure 48: Datasheet of Schott GG475 optical longpass filter

AR0135CS

1/3-inch 1.2 Mp CMOS Digital Image Sensor with Global Shutter

Description

The AR0135CS from ON Semiconductor is a 1/3-inch 1.2 Mp CMOS digital image sensor with an active-pixel array of 1280 (H) × 960 (V). It is designed for low light performance and features a global shutter for accurate capture of moving scenes and synchronization with pulsed light sources. It includes sophisticated camera functions such as auto exposure control, windowing, scaling, row skip mode, and both video and single frame modes. It is programmable through a simple two-wire serial interface. The AR0135CS produces extraordinarily clear, sharp images, and its ability to capture both continuous video and single frames makes it the perfect choice for a wide range of applications, including scanning and machine vision.

Table 1. KEY PERFORMANCE PARAMETERS

Parameter	Typical Value
Optical Format	1/3-inch (6 mm)
Active Pixels	1280 (H) × 960 (V) = 1.2 Mp
Pixel Size	3.75 μm
Color Filter Array	RGB Bayer, Monochrome
CRA	0°, 19°, 25°
Shutter Type	Global Shutter
Input Clock Range	6–50 MHz
Output Pixel Clock (Maximum)	74.25 MHz
Output Serial Parallel	 HiSPi 12-bit
Frame Rate Full Resolution 720p	 54 fps 60 fps
Responsivity (Under D65 with 670 nm IRCF) RGB Bayer Monochrome	 34 ke⁻/lux*sec 85 ke⁻/lux*sec
SNR_{MAX}	40.7 dB
Dynamic Range	71.1 dB
Supply Voltage I/O Digital Analog HiSPi	 1.8 or 2.8 V 1.8 V 2.8 V 0.4 V
Power Consumption	292 mW
Operating Temperature	–30°C to + 70°C (Ambient) –30°C to + 80°C (Junction)
Package Options	9 × 9 mm 63-pin IBGA
	Bare Die

ON Semiconductor®

www.onsemi.com

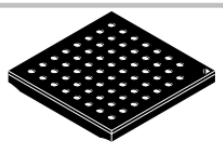

IBGA63 9 × 9
CASE 503AZ

ORDERING INFORMATION

See detailed ordering and shipping information on page 2 of this data sheet.

Features

- ON Semiconductor's Next Generation Global Shutter Technology
- Superior Low-light Performance
- HD Video (720p60)
- Video/Single Frame Mode
- Flexible Row-skip Modes
- On-chip AE and Statistics Engine
- Parallel and Serial Output
- Support for External LED or Flash
- Auto Black Level Calibration
- Context Switching

Applications

- Barcode Scanner
- 3D Scanning
- Positional Tracking
- Iris Scanning
- Augmented Reality
- Virtual Reality
- Biometrics
- Machine Vision
- Gesture Control

© Semiconductor Components Industries, LLC, 2016
April, 2017 – Rev. 6
1
Publication Order Number:
AR0135CS/D

Figure 49: Datasheet of CMOS sensor AR0135CS

TSH Test Cassette (Serum/Plasma)
Package Insert

A rapid test for detecting TSH quantitative in serum or plasma that with the use of Fluorescence Immunoassay Analyzer.

【INTENDED USE】

TSH Test Cassette (Immunofluorescence Assay) is intended for in vitro quantitative determination of Thyroid Stimulating Hormone (TSH) in serum, plasma. Measurement of TSH is useful to aid in the screening the adult population for primary hypothyroidism by medical professionals. It could also be used in screening neonates for hypothyroidism.

【SUMMARY】

Thyroid-stimulating hormone (also known as thyrotropin, thyrotropic hormone, TSH or hTSH for human TSH) is a pituitary hormone that stimulates the thyroid gland to produce thyroxine (T_4), and then triiodothyronine (T_3) which stimulates the metabolism of almost every tissue in the body.[1] It is a glycoprotein hormone synthesized and secreted by thyrotrope cells in the anterior pituitary gland, which regulates the endocrine function of the thyroid.[2][3] TSH (with a half life of about an hour) stimulates the thyroid gland to secrete the hormone thyroxine (T4), which has only a slight effect on metabolism. T4 is converted to triiodothyronine (T3), which is the active hormone that stimulates metabolism. About 80% of this conversion is in the liver and other organs, and 20% in the thyroid itself. [1] Laboratory testing of thyroid stimulating hormone* levels in the blood is considered the best initial test for hypothyroidism.[4] It is important to note the statement from the Subclinical Thyroid Disease Consensus Panel: "There is no single level of serum TSH at which clinical action is always either indicated or contraindicated. The higher the TSH, the more compelling is the rationale for treatment. It is important to consider the individual clinical context (e.g. pregnancy, lipid profile, ATPO antibodies)." [5]

【PRINCIPLE】

TSH Test Cassette is based on fluorescence immunoassay technology. TSH Test Cassette (Serum/Plasma) detects Thyroid Stimulating Hormone through immunochromatographic quantitative detection technology. The sample moves through the strip from sample pad to absorbent pad by the chromatographic force. If the test sample contains TSH, it attaches to the TSH antibody which is conjugated with fluorescent microspheres. Then the complex will be captured by the capture antibody coated on the nitrocellulose membrane (Test line). The concentration of TSH in the sample correlates linearly with the fluorescence signal intensity captured on the T line. According to the fluorescence intensity of the test and product standard curve, the concentration of TSH in the sample can be calculated by Analyzer to show TSH concentration in specimen.

【REAGENTS】

The test include TSH antibody coated particles and TSH antibody coated on the membrane.

【PRECAUTIONS】

1. For professional *in vitro* diagnostic use only.
2. Do not use after the expiration date indicated on the package. Do not use the test if the foil pouch is damaged. Do not reuse.
3. This test contains products of animal origin. Certified knowledge of the origin and/or sanitary state of the animals does not completely guarantee the absence of transmissible pathogenic agents. It is therefore recommended that these products be treated as potentially infectious, and handled observing usual safety precautions (e.g., do not ingest or inhale).
4. Avoid cross-contamination of specimens by using a new specimen collection container for each specimen obtained.
5. Do not eat, drink or smoke in the area where the specimens and tests are handled. Handle all specimens as if they contain infectious agents. Observe established precautions against microbiological hazards throughout the procedure and follow standard procedures for proper disposal of specimens. Wear protective clothing such as laboratory coats, disposable gloves and eye protection when specimens are assayed.
6. Do not interchange or mix reagents from different lots.
7. Humidity and temperature can adversely affect results.
8. Used testing materials should be discarded in accordance with local regulations.
9. Read the entire procedure carefully prior to any testing.
10. The TSH Test Cassette is only operational in the Analyzer. And tests should be applied by professionally trained staff working in certified laboratories at some remove from the patient and clinic at which the sample(s) is taken by qualified medical personnel.

【STORAGE AND STABILITY】

1. The test should be stored at 4-30 °C until the expiry date printed on the sealed pouch.
2. The test must remain in the sealed pouch until use.
3. **Do not freeze.**
4. Care should be taken to protect the components of the test from contamination.
5. Do not use if there is evidence of microbial contamination or precipitation. Biological contamination of dispensing equipment, containers or reagents can lead to false results.

【SPECIMEN COLLECTION AND PREPARATION】

Blood Sample Taking

1. Collect the specimens according to standard procedures.
2. Do not leave specimens at room temperature for prolonged periods. Serum and plasma specimens may be stored at 2-8 °C for up to 3 days, for long term storage, specimens should be kept below -20 °C.
3. Bring specimens to room temperature prior to testing. Frozen specimens must be completely thawed and mixed well prior to testing. Avoid repeated freezing and thawing of specimens.
4. EDTA, Heparin sodium, can be used as the anticoagulant tube for collecting the blood specimen.

Sample Dilution/Sample Stability

1. Transfer **75 µL of serum or plasma** to the buffer tube with the micro pipette.
2. Close the tube and shake the sample by hand forcefully for approximately **10 seconds** so sample and dilution buffer mix well.
3. Let the diluted sample rest for approximately **1 minute**.
4. The diluted sample can then be used immediately or stored for up to 8 hours.

【MATERIALS】

Materials Provided

- Test Cassettes
- ID Card
- Specimen Collection Tubes with buffer
- Package Insert

Materials Required But Not Provided

- Timer
- Centrifuge
- Fluorescence Immunoassay Analyzer
- Pipettes
- Specimen Collection Containers

【DIRECTIONS FOR USE】

Refer to Fluorescence Immunoassay Analyzer Operation Manual for the complete instructions on use of the Test. The test should be in room temperature.

Allow the test, specimen, buffer and/or controls to reach room temperature (15-30 °C) prior to testing.

1. Turn on the Analyzer power. Then according to the need, select "Standard test" or "Quick test" mode.
2. Remove the ID card and insert it into the Analyzer port.
3. **Serum or plasma:** Pipette **75 µL serum or plasma** into the buffer tube, mix the specimen and the buffer well.
4. **Add diluted specimen with a Pipette:** Pipette **75 µL** diluted specimen into the sample well. Start the timer at the same time.
5. There are two test modes for Fluorescence Immunoassay Analyzer, Standard Test mode and Quick Test mode. Please refer to the user manual of Fluorescence Immunoassay Analyzer for details.
   "Quick test" mode: Insert the test cassette into the Analyzer at **15 minutes** after sample application click **"QUICK TEST"**, fill the test information and click **"NEW TEST"** immediately, the Analyzer will automatically give the test result after a few seconds.
   "Standard test" mode: Insert the test cassette into the Analyzer immediately after sample application, click **"STANDARD TEST"**, fill the test information and click **"NEW TEST"** at the same time, the Analyzer will automatically counting down 15 **minutes**. After the countdown, the Analyzer will give the result at once.

【INTERPRETATION OF RESULTS】

Results read by Fluorescence Immunoassay Analyzer.

The result of tests for TSH is calculated by Fluorescence Immunoassay Analyzer and display the result on the screen. For additional information, please refer to the user manual of Fluorescence Immunoassay Analyzer.

Working range of **FIATEST ™** TSH is 0.1-100 µIU/mL.

【QUALITY CONTROL】

Each TSH Test Cassette contains internal control that satisfies routing quality control requirements. This internal control is performed each time a patient sample is tested. This control indicates that the test device was inserted and read properly by Fluorescence Immunoassay Analyzer. An invalid result from the internal control causes an error message on Fluorescence Immunoassay Analyzer indicating that the test should be repeated.

【LIMITATIONS】

1. The TSH Test Cassette (Serum/Plasma) is for professional in vitro diagnostic use. and should only be used for the quantitative detection of TSH.
2. The TSH Test Cassette (Serum/Plasma) will only indicate the presence of TSH antigen in the specimen and should not be used as the sole criteria for evaluating thyroid function.
3. As with all diagnostic tests, a confirmed diagnosis should only be made by a physician after all clinical and laboratory findings have been evaluated.
4. The results of Fluorescence Immunoassay Analyzer are only for the analysis of the results on the rapid tests. It should not be used as the sole criteria for treatment decisions. If the result is positive, other clinical findings and alternative test methods are recommended to reach proper medical treatments.

【EXPECTED RESULTS】

Concentrations	Clinical Reference
<20 µIU/mL	Normal Neonatal
<10 µIU/mL	Normal Children
<5 µIU/mL	Normal adult

【PERFORMANCE CHARACTERISTICS】

1. Accuracy

The test deviation ≤ ±15%.

2. Assay Range and Detection Limit

- Assay Range: 0.1-100 µIU/mL.
- Detection Limit (Analytical Sensitivity): 0.1 µIU/mL.

3. Linear range

0.1-100 µIU/mL, R≥0.990

4. Precision

Intra-lot precision

Within-run precision has been determined by using 10 replicates of 2 specimens containing 5.0 µIU/mL and 20 µIU/mL of TSH. C.V. is ≤ 15%.

Inter-lot precision

Between-run precision has been determined by using 10 replicates for each of three lots using 2 specimens containing 5.0 µIU/mL and 20 µIU/mL of TSH. C.V. is ≤15%.

5. Method comparation

The assay was compared with Roche electrochemical luminescence Assay test with 100 samples. The correlation coefficient(r) is 0.984.

【BIBLIOGRAPHY】

1. Merck Manual of Diagnosis and Therapy, Thyroid gland disorders.
2. The American Heritage Dictionary of the English Language, Fourth Edition. Houghton Mifflin Company. 2006. ISBN 0-395-82517-2.
3. Sacher R, Richard A. McPherson (2000). Widmann's Clinical Interpretation of Laboratory Tests, 11th ed. F.A. Davis Company. ISBN 0-8036-0270-7.
4. So, M; MacIsaac, RJ; Grossmann M (August 2012). "Hypothyroidism". Australian Family Physician 41 (8): 556–62.
5. Surkset. al.,JAMA 291:228, 2004.

CE

Figure 50: Package insert of AllTest TSH Test